Bryn Mawr College

Scholarship, Research, and Creative Work at Bryn Mawr College

Biology Faculty Research and Scholarship

Biology

2022

Towards mapping biodiversity from above: Can fusing lidar and hyperspectral remote sensing predict taxonomic, functional, and phylogenetic tree diversity in temperate forests?

Aaron G. Kamoske
Michigan State University

Kyla M. Dahlin
Michigan State University

Quentin D. Read
National Socio-Environmental Synthesis Center

Sydne Record
Bryn Mawr College, srecord@brynmawr.edu
Follow this and additional works at: https://repository.brynmawr.edu/bio_pubs

Scott C. Stark
Michigan State University
Part of the Biology Commons

Citation

Authors

Aaron G. Kamoske, Kyla M. Dahlin, Quentin D. Read, Sydne Record, Scott C. Stark, Shawn P. Serbin, and Phoebe L. Zarnetske

RESEARCH ARTICLE

Towards mapping biodiversity from above: Can fusing lidar and hyperspectral remote sensing predict taxonomic, functional, and phylogenetic tree diversity in temperate forests?

Aaron G. Kamoske[1,2] | Kyla M. Dahlin[1,3] | Quentin D. Read[4] | Sydne Record[5] | Scott C. Stark[6] | Shawn P. Serbin[7] | Phoebe L. Zarnetske[3,8]

[1]Department of Geography, Environment, & Spatial Sciences, Michigan State University, East Lansing, Michigan, USA

[2]USDA Forest Service, Geospatial Technology and Applications Center, Salt Lake City, Utah, USA

[3]Program in Ecology, Evolution, and Behavior, Michigan State University, East Lansing, Michigan, USA

[4]National Socio-Environmental Synthesis Center, Annapolis, Maryland, USA

[5]Department of Biology, Bryn Mawr College, Bryn Mawr, Pennsylvania, USA

[6]Department of Forestry, Michigan State University, East Lansing, Michigan, USA

[7]Environmental and Climate Sciences Department Upton, Brookhaven National Laboratory, New York, New York, USA

[8]Department of Integrative Biology, Michigan State University, East Lansing, Michigan, USA

Correspondence
Aaron G. Kamoske, Department of Geography, Environment, & Spatial Sciences, Michigan State University, East Lansing, MI, USA.
Email: kamoskea@msu.edu

Abstract

Aim: Rapid global change is impacting the diversity of tree species and essential ecosystem functions and services of forests. It is therefore critical to understand and predict how the diversity of tree species is spatially distributed within and among forest biomes. Satellite remote sensing platforms have been used for decades to map forest structure and function but are limited in their capacity to monitor change by their relatively coarse spatial resolution and the complexity of scales at which different dimensions of biodiversity are observed in the field. Recently, airborne remote sensing platforms making use of passive high spectral resolution (i.e., hyperspectral) and active lidar data have been operationalized, providing an opportunity to disentangle how biodiversity patterns vary across space and time from field observations to larger scales. Most studies to date have focused on single sites and/or one sensor type; here we ask how multiple sensor types from the National Ecological Observatory Network's Airborne Observation Platform (NEON AOP) perform across multiple sites in a single biome at the NEON field plot scale (i.e., 40 m × 40 m).

Location: Eastern USA.

Time period: 2017–2018.

Taxa studied: Trees.

Methods: With a fusion of hyperspectral and lidar data from the NEON AOP, we assess the ability of high resolution remotely sensed metrics to measure biodiversity variation across eastern US temperate forests. We examine how taxonomic, functional, and phylogenetic measures of alpha diversity vary spatially and assess to what degree remotely sensed metrics correlate with in situ biodiversity metrics.

Results: Models using estimates of forest function, canopy structure, and topographic diversity performed better than models containing each category alone. Our results show that canopy structural diversity, and not just spectral reflectance, is critical to predicting biodiversity.

Main conclusions: We found that an approach that jointly leverages spectral properties related to leaf and canopy functional traits and forest health, lidar derived

estimates of forest structure, fine-resolution topographic diversity, and careful consideration of biogeographical differences within and among biomes is needed to accurately map biodiversity variation from above.

1 | INTRODUCTION

A fundamental goal in community ecology is to understand and predict the spatial distributions of species, traits, and biodiversity across ecosystems (Keddy, 1992). However, taxonomic, functional, and phylogenetic dimensions of biodiversity address different ecological questions. Taxonomic diversity counts the number of species or taxa in an area and their relative abundance and can therefore be related to hypotheses about community assembly (Chase, 2010). Functional diversity quantifies the range of functional variation (e.g., leaf nutritional or physiological properties, shade tolerance, canopy height, leaf area) in an area, and studies have shown that higher functional diversity is associated with more resilient (Schmitt et al., 2019) and productive ecosystems (Roscher et al., 2012). Phylogenetic diversity measures the relatedness of species within an area and is therefore related to the evolutionary history of a landscape and its occupants (Morlon et al., 2010; Srivastava et al., 2012).

Each dimension of biodiversity may be driven by distinct abiotic and biotic factors and ecological processes, while following unique spatial and temporal patterns (Gaston, 2000; Lomolino et al., 2010). For example, tree taxonomic diversity is affected by biotic interactions, environmental drivers and change, as well as homogenization due to management practices and disturbance regimes (Baiser et al., 2012; Li et al., 2020; Olden & Rooney, 2006). Plant functional diversity is critical for determining biodiversity–ecosystem function relationships (Baiser & Lockwood, 2011; Flynn et al., 2011) and is driven by niche availability, community assembly, and interactions with species at higher trophic levels (Petchy & Gaston, 2006). Phylogenetic diversity is influenced by the spatial clustering of closely related species that occupy similar environments and is driven by long-term biogeographical processes (Cavender-Bares et al., 2009).

The influence of these different dimensions of biodiversity on the observable properties of forest canopies is not well known, but is critical to characterize because forest canopies link the atmosphere and the vast majority of Earth's terrestrial biomass (Bonan, 2008; Ozanne et al., 2003), provide key ecosystem services such as carbon sequestration (Bunker et al., 2005; Hooper et al., 2012; Isbell et al., 2015), and are impacted by rapid global change (e.g., Brook et al., 2008; Cardinale et al., 2012; Parmesan & Yohe, 2003; Urban, 2015). Because different dimensions of biodiversity may reflect specific drivers of ecosystem functioning and respond to global change in unique ways, a multidimensional approach is essential to better understand the emergent response of ecosystems and plant biodiversity to these drivers.

Much of the current understanding of the spatial distribution of dimensions of biodiversity at broad spatial extents has come from coarse spatial grain (30 m and greater) satellite remote sensing products (Bush et al., 2017; Duro et al., 2007; Pettorelli et al., 2014; Skidmore et al., 2021; Turner et al., 2003). For example, remotely sensed products have helped clarify the scale-dependence of variation in topography and biogeography as drivers of patterns of tree biodiversity (Read et al., 2019; Record et al., 2020; Zarnetske et al., 2019). Even though remote sensing products capable of providing standardized measurements for the investigation of vegetation function and diversity have been available over a range of spatial scales for decades (He et al., 2015), ecologists still heavily rely on ground-based biodiversity observations due to differences in scale between individual organisms and remotely sensed products (Tews et al., 2004). Ecological observations at coarse spatial grains can lead to dominant landscape features homogenizing measurements (Boyce, 2006; Cooper et al., 2019), leading to the omission of fine-scale heterogeneity and patterns, which can significantly impact the characterization of ecosystem functioning.

Fine-resolution airborne remote sensing platforms are transforming the spatial scale of observation (< 30 m) and may help resolve scale mismatches between field observations and the estimation of vegetation diversity at larger spatial extents. The National Ecological Observatory Network's Airborne Observation Platform (NEON AOP) simultaneously collects both passive optical high spectral resolution imaging spectroscopy, or 'hyperspectral' (e.g., 380–2,500 nm; 5-nm bands), and active lidar measurements of canopy optical and structural properties (Kampe et al., 2010). These data are collected near-annually at a network of 81 systematically sampled sites across the United States with ground data at individual field plots within the remote sensing footprint (Barnett et al., 2019; Kampe et al., 2010; Thorpe et al., 2016). Airborne lidar has been used to measure metrics critical to mapping biodiversity across landscapes, such as the structural diversity of forests (e.g., Cosovic et al., 2020; Kamoske et al., 2019; Shao et al., 2019; Stark et al., 2015) and topographic diversity (Dahlin et al., 2012). Similarly, hyperspectral imagery has been used to measure the spectral diversity of ecosystems at fine spatial scales, which can be related to plant biodiversity (Cavender-Bares et al., 2017; Dahlin, 2016; Gholizadeh et al., 2019; Laliberté et al., 2020; Wang & Gamon, 2019). Hyperspectral and lidar fusion, or the combination of these two data types through statistical analyses for deeper understanding of landscape properties, allows for the detection of more subtle variations within forest types than using either sensor type alone (Dalponte et al., 2008).

While enthusiasm for the application of hyperspectral and lidar remote sensing to map biodiversity has grown in recent years (Jetz et al., 2019; Stavros et al., 2017), most studies have focused on within-site diversity mapping in a single site using hyperspectral imagery (Dahlin, 2016; Gholizadeh et al., 2018, 2019; Wang et al., 2018) or cross-site studies focused on lidar (Gough et al., 2020). Yet, to operationalize a biodiversity mapping program (e.g., the Group on Earth Observations' Biodiversity Observation Networks'' Essential Biodiversity Variables; Jetz et al., 2019; Skidmore et al., 2021), methods must work across multiple sites and biomes and address various dimensions of biodiversity. Resolving relationships between different types of canopy observations and different dimensions of biodiversity within and among ecosystems is essential to advance our understanding of the patterns of and changes in biodiversity as well as the nature of diversity–function relationships (LaRue et al., 2019).

In this study, we focus on the variation in these three dimensions of alpha diversity at multiple NEON sites across a broad (10°) latitudinal gradient of temperate forests. We address three questions critical to understanding forest biodiversity in this temperate forest latitudinal gradient: (a) How do these different dimensions of biodiversity vary within and among these forest regions? (b) Which remotely sensed metric, or combination of metrics, best predicts alpha taxonomic, functional, and phylogenetic diversity across a latitudinal gradient of temperate forest regions? and (c) Are predictions universal, or does incorporating information about the abiotic environment and geography improve estimates? We hypothesized that taxonomic and functional diversity would decrease with increasing latitude, as more southern sites are 'older' due to their lack of glaciation and the prevalence of these patterns globally (e.g., Kreft & Jetz, 2007; Swenson et al., 2011). In contrast, we expected phylogenetic diversity would increase with latitude as more seasonal variation would lead to more competitive advantages for gymnosperms based on the literature (e.g., Massante et al., 2019). We also expected that remotely sensed vegetation information would be able to capture the variation in these dimensions of biodiversity without the need for additional environmental information, as has been suggested in the remote sensing literature (e.g., Meireles et al., 2020; Skidmore et al., 2021).

2 | MATERIALS AND METHODS

2.1 | Study sites

Field measurements and remote sensing data were acquired from five climatically and ecologically diverse NEON sites located along a latitudinal gradient of eastern US temperate forests (Figure 1). These sites include, from south to north, Talladega National Forest (TALL), Oak Ridge National Laboratory (ORNL), Mountain Lake Biological Station (MLBS), the Smithsonian Environmental Research Center (SERC), and Harvard Forest (HARV). Though all temperate forests, these forests are from multiple forest regions (e.g., Dyer, 2006; Southern mixed oak-pine, mesophytic Appalachian

oaks, Oak-hickory, Northern hardwoods). Across all sites, mean annual precipitation ranges from 967 to 1,350 mm, mean annual temperature ranges from 8 to 17 °C, mean canopy height ranges from 18 to 38 m, elevation ranges from 15 to 1,126 m, and airborne imagery collection extents range from 110–355 km^2 (Appendix A).

2.2 | Calculating tree diversity metrics within NEON field plots

To quantify tree taxonomic, functional, and phylogenetic diversity at the NEON plot scale (i.e., 40 m × 40 m), we downloaded woody-plant species data from the NEON data portal (National Ecological Observatory Network, 2020) for the same year that the NEON AOP flights and our fieldwork were conducted (i.e., 2018 for all sites, except 2017 for SERC) and filtered it to retain only living trees. We then used the stem diameters of each individual tree to calculate the relative abundance of each species per plot by summing the total basal area of each species and dividing it by the total basal area of all species in each plot (Auclair & Cottam, 1971; Whitehead, 1978). We elected to use basal area, instead of individual or stem count, for relative abundance to generate metrics more similar to the remotely sensed data; for example, we would expect a plot dominated by a few large trees to be more spectrally and structurally homogeneous than a plot composed of the same number of stems, but a more even size distribution. To quantify alpha taxonomic diversity within each field plot we used these relative abundance values to calculate Shannon's diversity index (Spellerberg & Fedor, 2003). To calculate phylogenetic and functional diversity, we compiled functional trait data from two sources: the TRY-db trait database (Kattge et al., 2020) and a compilation of published trait values for North American tree species (Stevens et al., 2020). We used a published tree species phylogeny (Potter & Koch, 2014; Potter & Woodall, 2012) that includes all species present in the field plots described above. We calculated abundance-weighted phylogenetic and functional diversity metrics using basal area to represent species abundances (Appendix B). We resolved any discrepancies in species names using the most recent taxonomy listed by the International Union for Conservation of Nature and Natural Resources (IUCN; http://iucnredlist.org). Since some species had at least one missing functional trait value (~15% of species for most traits; Appendix H), we used the phylogeny to impute the missing values, assuming an Ornstein–Uhlenbeck evolutionary model. We imputed the missing data using the phylopars function from the *Rphylopars* R package (Goolsby et al., 2017; R Core Team, 2021). Next, we created a Gower distance matrix of normalized functional traits using the imputed trait dataset and phylogeny for all the species (Read et al., 2019). We then created a cophenetic distance matrix based on the tree species phylogeny data. Next, we calculated a community-level mean pairwise distance (MPD) metric for both functional and phylogenetic datasets. While there are many different methods to calculate taxonomic, functional, and phylogenetic diversity (Jost, 2006, 2007), we used the above metrics because they are widely used and easily interpreted. Furthermore,
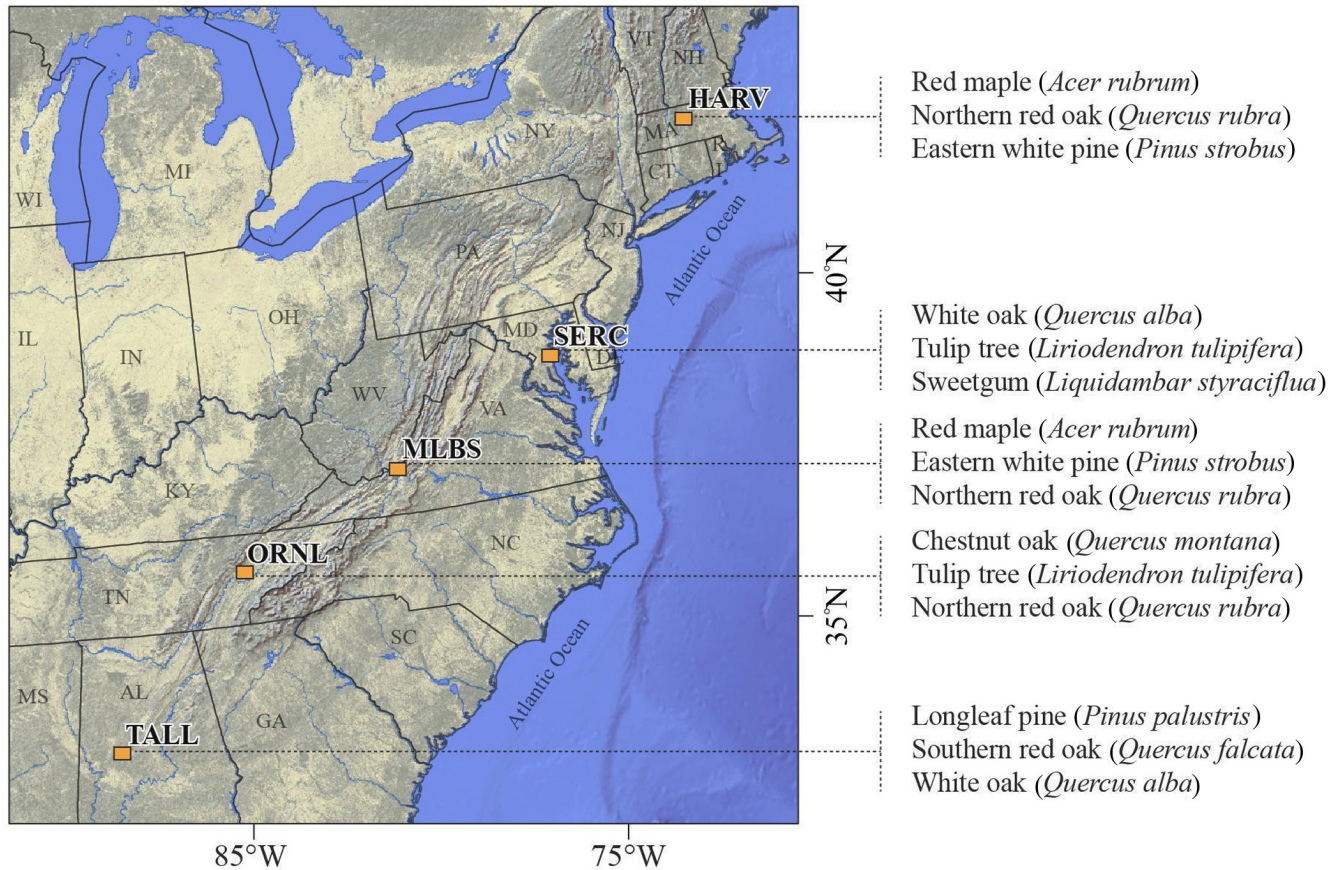
FIGURE 1 Map showing National Ecological Observatory Network (NEON) field sites used in this study (orange squares) and the three most common tree species for each site based on NEON field observations. Individual site information and abbreviations found in Appendix A

the metrics we used average all pairwise distances so that very distantly related, or functionally distinct species pairs, are more heavily weighted (Read et al., 2019). Because these diversity metrics increase when distantly related or highly functionally disparate species pairs co-occur, they tend to emphasize functionally relevant differences.

Several of the plots only had one species present, thus we could not calculate functional and phylogenetic diversity metrics at those plots (Read et al., 2019). After removing these from the dataset, there were 19 plots for TALL, 14 plots for ORNL, 32 plots for MLBS, 14 plots for SERC, 17 plots for HARV, and 96 plots overall.

2.3 | Remote sensing data

To better understand the role of canopy observations on different dimensions of biodiversity we processed airborne lidar and hyperspectral data (e.g., 1-m spatial resolution) from the NEON AOP into 43 metrics related to spectral diversity, vegetation health, canopy structure, and topography (Appendices C–E, respectively). All remotely sensed data were collected during peak greenness as defined by Moderate Resolution Imaging Spectroradiometer normalized difference vegetation index (NDVI) (Kampe et al., 2010). Two different

lidar systems operated at the same specifications were used for these collections (Appendix A; Kamoske et al., 2019).

2.4 | Forest structural and topographic diversity from lidar remote sensing

To calibrate lidar structural diversity estimates with Beer–Lambert extinction coefficients, we collected hemispherical photographs across each site at locations representing the diversity of tree species and stand structures in conjunction with NEON AOP flights following the methodology outlined in Kamoske et al. (2019). This method entailed taking hemispherical photographs in at least 10 plots, with four photographs each, representing the diversity of species and stand types at each site. We then calculated plant area index [e.g., hereafter referred to as leaf area index (LAI); Miller, 1967], which is widely used as a proxy for LAI due to the difficulty of correcting for non-foliage elements (Richardson et al., 2009), using the DIGITAL HEMISPHERICAL PHOTOGRAPHY software (DHP; Leblanc et al., 2005) and setting the zenith angle to match the scanning angle of each lidar sensor (Appendix A; Korhonen et al., 2011; Richardson et al., 2009; Sabol et al., 2014; Solberg et al., 2006). Because this approach relied on our own field data

KAMOSKE ET AL.

Global Ecology
and Biogeography

A Journal of
Macroecology

WILEY 5

collection, the number of NEON sites used was limited by our field campaign. NEON does collect hemispherical photographs; however, these did not meet our data quality standards for LAI estimation.

To estimate three-dimensional canopy structural diversity, we processed the lidar data for leaf area density (LAD; the total leaf area per unit of volume) at a 10 m × 10 m spatial resolution using our *canopyLazR* R package (Kamoske et al., 2019; http://github.com/akamoske/canopyLazR), which is similar to other published methods (MacArthur & Horn, 1969; Solberg et al., 2006; Stark et al., 2012; Sumida et al., 2009; Zhao & Popescu, 2009). First, we normalized the point cloud to height above the ground and then calculated LAD by counting the number of lidar pulses that enter and exit each voxel in each vertical column of data that has at least one ground return. Due to this relatively coarse lidar data exhibiting noise caused by topographic variation in the LAD results and to have an easily comparable dataset, we removed the LAD estimates from the bottom 5 m of the canopy (Kamoske et al., 2019). We then calibrated the LAD estimates for each individual site using a Beer–Lambert extinction coefficient derived by calculating the slope of a regression equation between hemispherical photograph derived LAI and lidar estimated LAI (e.g., Appendix F; Richardson et al., 2009; Sabol et al., 2014). To remove non-forest pixels, we applied a canopy height and LAI mask to the upper end of each LAD dataset using Tukey's outlier test ($k = 1.5$) and then removed all pixels where LAI equalled zero (Kamoske et al., 2019). With these masked LAD rasters, we calculated 21 forest structural metrics at a 10 m × 10 m resolution for each field plot (Appendix D). To quantify topographic diversity at each site, we calculated nine variables using QGIS (QGIS, 2022) and the 10 m × 10 m lidar derived digital terrain model (Appendix E).

2.5 | Hyperspectral remote sensing reflectance metrics

We processed the atmospherically corrected hyperspectral imagery from the NEON AOP before analysis using our *hypRspec* R package on GitHub (Kamoske et al., 2020; http://github.com/akamoske/hypRspec). After removing all flight lines re-flown due to cloudiness, we visually identified noisy bands in the data (e.g., moisture and atmospheric absorption) and removed all wavelengths that were below 500 nm, between 1,350 and 1,450 nm, between 1,800 and 2,000 nm, and above 2,400 nm. We then calculated a narrowband NDVI mask (red = 674 nm; nir = 830 nm; NDVI > .5) to remove all unlikely-to-be-vegetated pixels from further analysis (Dahlin et al., 2014). To remove all shaded pixels, to maintain consistent conditions between pixels, we used Tukey's outlier test ($k = 1.5$) where all pixels that had a reflectance below the lower threshold were considered outliers and removed (Kamoske et al., 2020). We then applied a topographic correction to reduce the effects of terrain, view, and illumination (Soenen et al., 2005) and a bidirectional reflectance distribution function effects correction (BRDF) with a thick Ross kernel and a dense Li kernel to remove the anisotropic

scattering properties of vegetation that result in flight line artifacts (Colgan et al., 2012; Collings et al., 2010; Schlapfer et al., 2015; Wang et al., 2020; Wanner et al., 1995; Weyermann et al., 2015).

Using this corrected hyperspectral data, we calculated 13 hyperspectral reflectance and principal component analysis (PCA) derived metrics (Appendix C) by extracting reflectance spectra from all pixels within each field plot and using the mean value if a pixel occurred in multiple flight lines. To calculate the PCA based metrics, which were used to capitalize on the reflectance across all wavelengths, we used the extracted data from all plots as a single dataset and PCA to reduce the dimensionality of this subset of the data (Venables & Ripley, 2002). We used the first two principal components (PCs), which captured 97.6% of the overall variation in the plot spectra, in subsequent analyses. We elected not to include remotely sensed estimates of plant traits (e.g., Wang et al., 2020) as these were not available for all our study sites at the time of the analysis, and recent work has suggested that NEON-produced trait estimates do not necessarily reflect on-the-ground measurements (Pau et al., 2021).

2.6 | Influence of biodiversity on remote sensing metrics

In total, we had 43 possible predictor metrics. We calculated each metric at its nominal resolution, and then aggregated the results to produce a single value for each NEON plot (i.e., 40 m × 40 m), calculating the mean, minimum, maximum, range, and standard deviation of each metric that did not already produce a single value (e.g., convex hull volume). This resulted in 191 possible predictors overall. To quantify the relative importance of these metrics related to the structural, spectral, and topographic heterogeneity of eastern temperate forests for different dimensions of alpha diversity we used a combination of linear mixed effect (LME) modelling (Gotelli & Ellison, 2013; Pinheiro & Bates, 2000) and stepwise Akaike information criterion (AIC) model selection (Burnham et al., 2011; Mascaro et al., 2011). To allow for direct comparison between model coefficients, we standardized all metrics and the three diversity variables (Gelman, 2008; mean = 0, $SD = .5$).

For each dimension of biodiversity, we calculated a single LME model for each predictor type individually (i.e., hyperspectral, lidar, and topography) and a single mixed effects model with all predictors combined. To avoid multicollinearity (e.g., Pearson's $R > .5$) we first tested the correlation between each pair of predictor variables and kept the variable most correlated with each dimension of biodiversity for further analysis. Using the remaining variables, we then developed an LME model using each of these variables as a fixed effect and site (e.g., TALL, ORNL) as a random effect to allow for inferences to extend to differences between sites in general rather than between the five sites for which we had data (Gotelli & Ellison, 2013; Pinheiro & Bates, 2000). We included these site level differences to help account for critical large-scale biogeographical and management differences between sites (Bengtsson et al., 2000; Dambrine et al., 2007; Dupouey et al., 2002; Reich et al., 2001).

We then used stepwise AIC model selection to determine the best combination of predictor variables for each model (Safken et al., 2021). We tested backward, forward, and bidirectional stepwise variable selection, all of which resulted in the same predictor variables for each model. We then removed any remaining variables with non-significant coefficients ($p > .05$) and evaluated final LME models with site as a random effect. Lastly, we performed LME partial regression analysis using the final metrics in each model grouped by type (i.e., hyperspectral, lidar, and topography) to determine the proportion of the final model's R^2 value assigned to each group of metrics (i.e., metric R^2/final model R^2).

We also tested the individual correlations between remote sensing metrics used in each final model and the associated biodiversity variable to better understand the relationship between biodiversity and individual observable canopy properties.

3 | RESULTS

3.1 | Variation of biodiversity and remote sensing metrics

In sites with spatially distinct broadleaf and needleleaf stands (i.e., TALL, HARV) there was more variability of spectral and structural diversity metrics compared to sites dominated by broadleaf species (i.e., SERC, ORNL, and MLBS; Figure 2). However, topographic variables did not follow these same patterns. Functional diversity variation was uniform among sites, but phylogenetic diversity was more variable within mixed forest sites (i.e., TALL and HARV) compared to the other broadleaf dominated sites (Figure 2). Moreover, the three dimensions of biodiversity were highly variable within each site, meaning that there are high and low diversity plots within each site, not a distinct latitudinal gradient as we hypothesized.

Furthermore, there were no strong linear relationships between remotely sensed metrics found in the final model and the associated dimension of biodiversity, with the highest significant R^2 just .19 (Figure 3). Lidar-derived metrics related to forest structure showed both positive and negative correlations in varying degrees, with hyperspectral and topographic metrics following the same pattern. Also, none of the individual metrics found in the final models had strong correlations to the biodiversity metrics.

3.2 | LME models

Models that included metrics derived from all three predictor types (i.e., hyperspectral, lidar, and topography) performed better than each individual predictor type (Figure 4; Table 1). In the best performing models, fixed effects explained all the variation in the taxonomic and functional diversity models, whereas random effects (i.e., site) had the largest influence on the phylogenetic model with the model R^2 increasing from .33 to .70 with the inclusion of
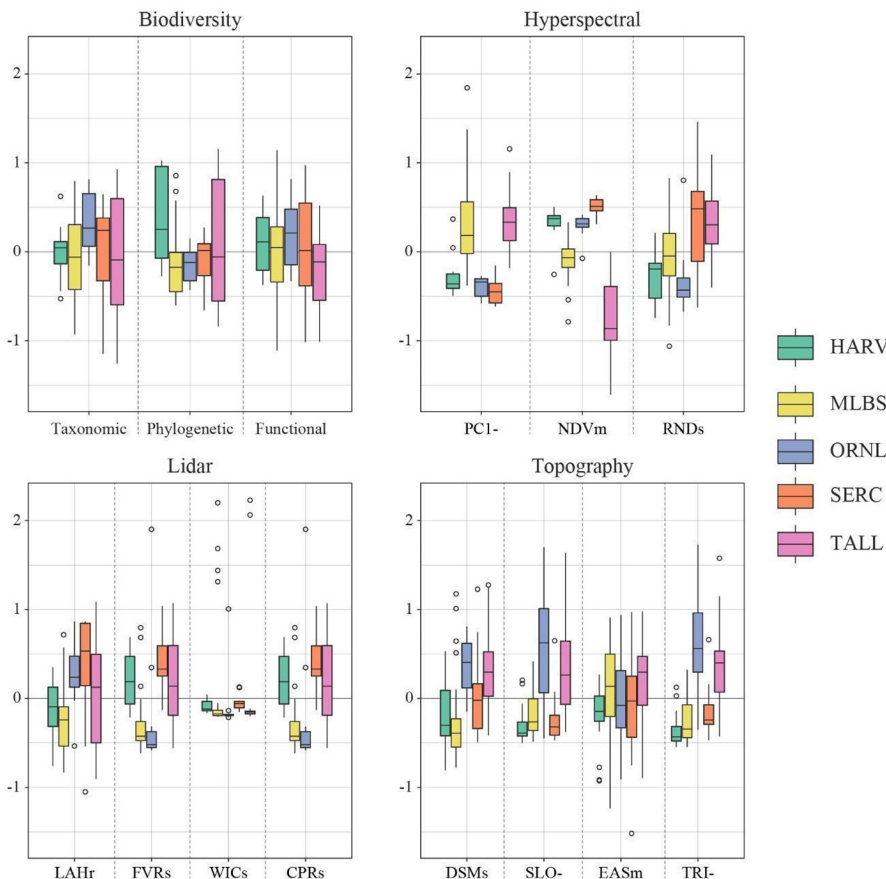
FIGURE 2 Boxplots showing variation of normalized metrics used in final linear mixed effect (LME) models. Metric abbreviations found in Table 1, with the last symbol signifying mean (m), minimum (−), range (r), or standard deviation (s). Site abbreviations found in Section 2.1 and Appendix A. Coloured bar plots show the interquartile range, solid horizontal lines are medians, vertical lines show largest and smallest value within 1.5 times the interquartile range, outliers are indicated with open circles
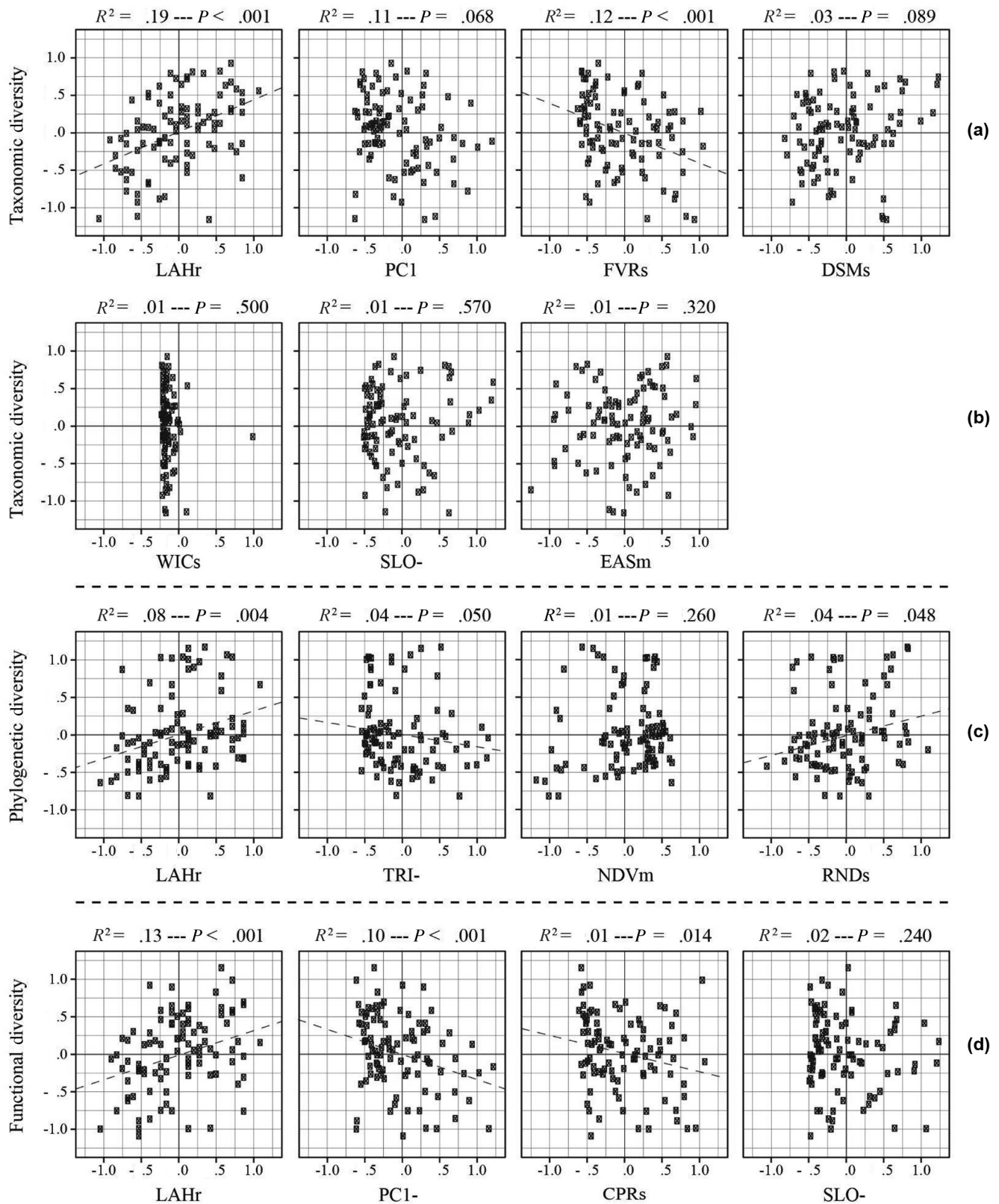
FIGURE 3 Boxes show the correlation between each diversity metric and remotely sensed metric; abbreviations for each metric and for site names are found in Table 1 and Appendix A, respectively, with the last symbol signifying mean (m), minimum (−), range (r), or standard deviation (s). Adjusted R^2 and p-values are listed above each plot and normalized values for each metric were used. Dotted lines show lines of best fit for all significant ($p < .05$) correlations
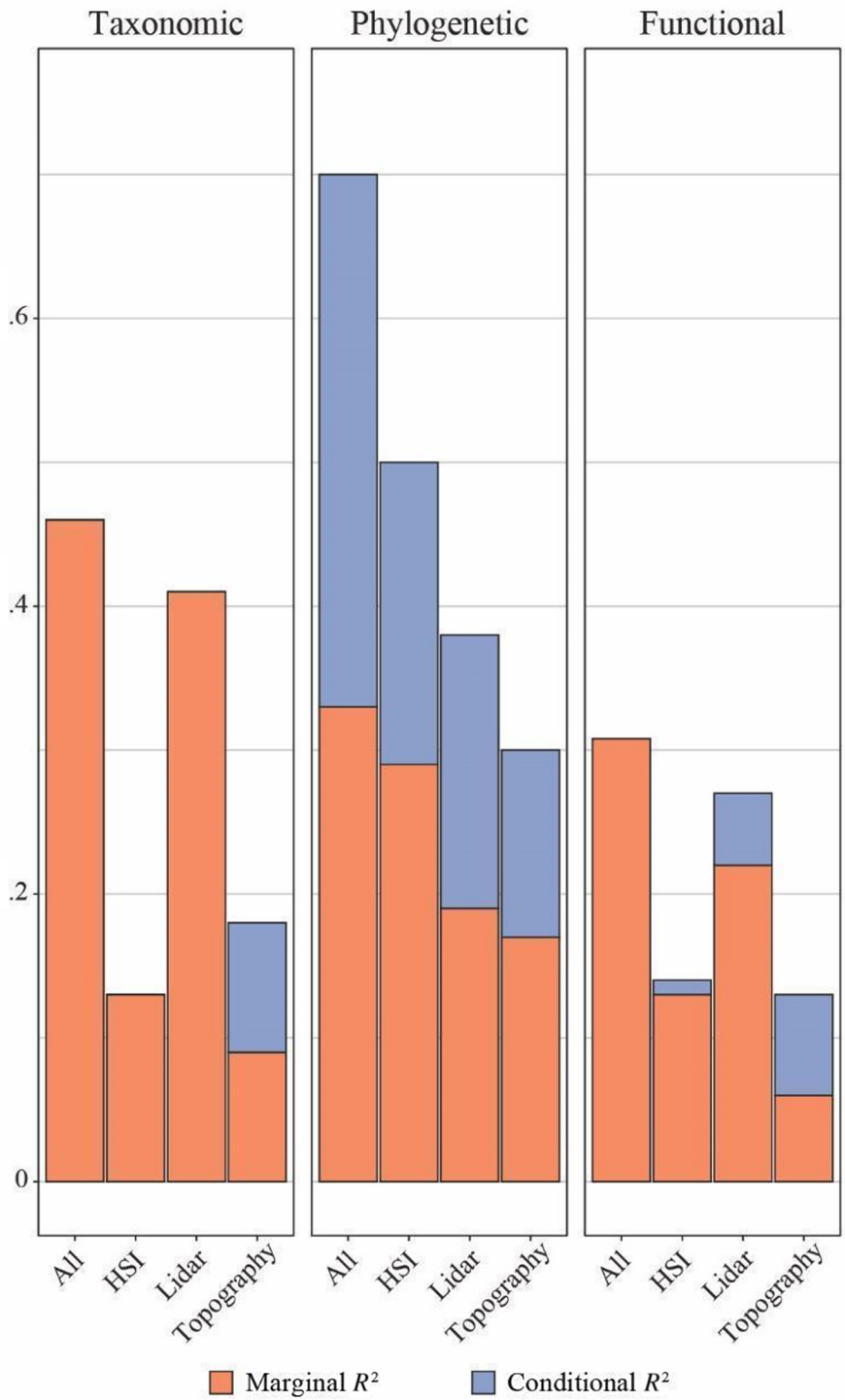
FIGURE 4 Marginal (only fixed effects, i.e., remote sensing-based metrics) and conditional (fixed and random effects, i.e., broader site-level differences) R^2 values for each model representing each sensor individually and all sensors combined. On the x axis, All refers to models utilizing hyperspectral (HSI), lidar (forest structure), and topographic metrics; HSI refers to models with only hyperspectral metrics; Lidar refers to models with only lidar derived metrics related to forest structure; and Topography refers to models with only topographic metrics

site (Table 1). This influence of site on phylogenetic diversity may be related to the inclusion of both conifer and broadleaf species, compared to sites that only have broadleaf species. The three best models included significant hyperspectral, lidar, and topographic metrics (Table 1); however, of the individual models, lidar explained the most taxonomic and functional diversity variation (Appendix G), showing the importance of relationships between forest structure and different dimensions of biodiversity. Given the improved model performance using all three predictor types in a single model, with higher R^2s and lower AICs (Appendix G), we used these full models

to further examine the ability to predict different dimensions of biodiversity.

To further understand model performance, we examined observed versus predicted plots, residuals, normalized coefficient values, and the performance of each group of metrics in the final models (Figure 5). All models showed randomly dispersed residuals that were not clustered by functional group (i.e., broadleaf, needle-leaf, or mixed forest) or by site (Figure 5b; Appendix G). All models included the range of maximum LAD heights within a plot metric, an important variable from Hardiman et al. (2011) that describes 3-D

TABLE 1 Final linear mixed effect (LME) model results, showing marginal R^2, conditional R^2, and relative RMSE

	Marginal R^2	Conditional R^2	Root Mean Square Error (RMSE)	Type	Variable	Abbreviation
Taxonomic diversity	.46	.46	.36	Lidar	Maximum leaf area density height	LAH
					Within canopy rugosity	WIC
					Canopy filled voxel ratio	FVR
				Topography	Eastness	EAS
					Digital surface model	DSM
					Slope	SLO
				Hyperspectral	Principal component 1	PC1
Phylogenetic diversity	.33	.70	.36	Lidar	Maximum leaf area density height	LAH
				Topographic	Topographic roughness index	TRI
				Hyperspectral	Normalized difference vegetation index	NDV
					Red-edge normalized difference vegetation index	RND
Functional diversity	.31	.31	.41	Lidar	Maximum leaf area density height	LAH
					canopy porosity ratio	CPR
				Topographic	Slope	SLO
				Hyperspectral	Principal component 1	PC1

Note: Only airborne remote sensing derived predictor variables used in final models are shown. Metrics may include range, minimum, maximum, mean, or standard deviation found within each National Ecological Observatory Network (NEON) plot, where appropriate, and are signified as such in the figures and appendices All metrics calculated in this study with definitions and references can be found in Appendices C–E.

canopy structural diversity, and several of the models included similar metrics (i.e., minimum slope and the minimum first PC). Moreover, metrics representing an individual sensor type were not universally positive or negative, instead showing a wide range of influence on each of the final models (Figure 5c; Appendix G). Within the final taxonomic and functional diversity models, lidar metrics had the largest influence, representing 65 and 52% of the total model R^2, respectively, while site had the largest influence on the phylogenetic model, representing 60% of the total model R^2 (Figure 5d).

4 | DISCUSSION

We used airborne remote sensing to measure different dimensions of biodiversity across eastern US temperate forest ecosystems, showing that spectral diversity, canopy structural heterogeneity, and topography together can explain a substantial amount of the variation in biodiversity dimensions within and across sites. Importantly, our results show that remotely sensed metrics derived from lidar and hyperspectral sensors vary in their ability to capture in situ measurements of biodiversity from field plots in these forested sites. Many studies have used hyperspectral (Asner & Martin, 2016; Cavender-Bares et al., 2016; Feret & Asner, 2014) or lidar (Bergen et al., 2009; Cosovic et al., 2020; Simonson et al., 2012) data to measure biodiversity in a range of ecosystems; however, far fewer have combined these data (Leutner et al., 2012; Zhao et al., 2018). While most of these studies have focused on taxonomic diversity or leaf functional traits, we show that an integration of lidar and hyperspectral remote

sensing data can be used to explain variation in multiple dimensions of alpha diversity.

To estimate biodiversity across temperate forests, an approach that jointly leverages spectral properties related to leaf and canopy functional traits and forest health, lidar derived estimates of forest structure, and fine-resolution topographic diversity is needed; approaches that focus on a single or subset of these categories will likely fall short. To this end, our models included hyperspectral derived metrics (Appendix C) related to a canopy's spectral reflectance in the visible, near-infrared, and shortwave-infrared wavelengths [i.e., principal component 1 (PC1); Oldeland et al., 2010], vegetation greenness [i.e., normalized difference vegetation index (NDVI); Rouse et al., 1974], and the red-edge, which has been shown to be critical to mapping vegetation health [red edge normalized difference vegetation index (RND); Gitelson & Merzlyak, 1994]. These models also included lidar derived metrics (Appendix D) related to the location within a canopy where the most leaf material occurs [i.e., mean leaf area density height (LAM); Hardiman et al., 2013], the ratio of the canopy that contains plant material [i.e., canopy filled voxel ratio (FVR); Hardiman et al., 2013], the relationship between the distribution of leaf material within a canopy and near-by canopies [i.e., within canopy rugosity (WIC); Hardiman et al., 2011], and the ratio of the canopy that does not contain plant material [i.e., canopy porosity ratio (CPR); Hardiman et al., 2013]. Lastly, topographic metrics (Appendix E) that were significant in our final models included elevation of all objects [i.e., digital surface model (DSM)], slope (SLO), how eastward a pixel's slope is facing [i.e., eastness (EAS)], and the difference in elevation between a central cell and its surrounding cells [i.e., topographic roughness index (TRI)].
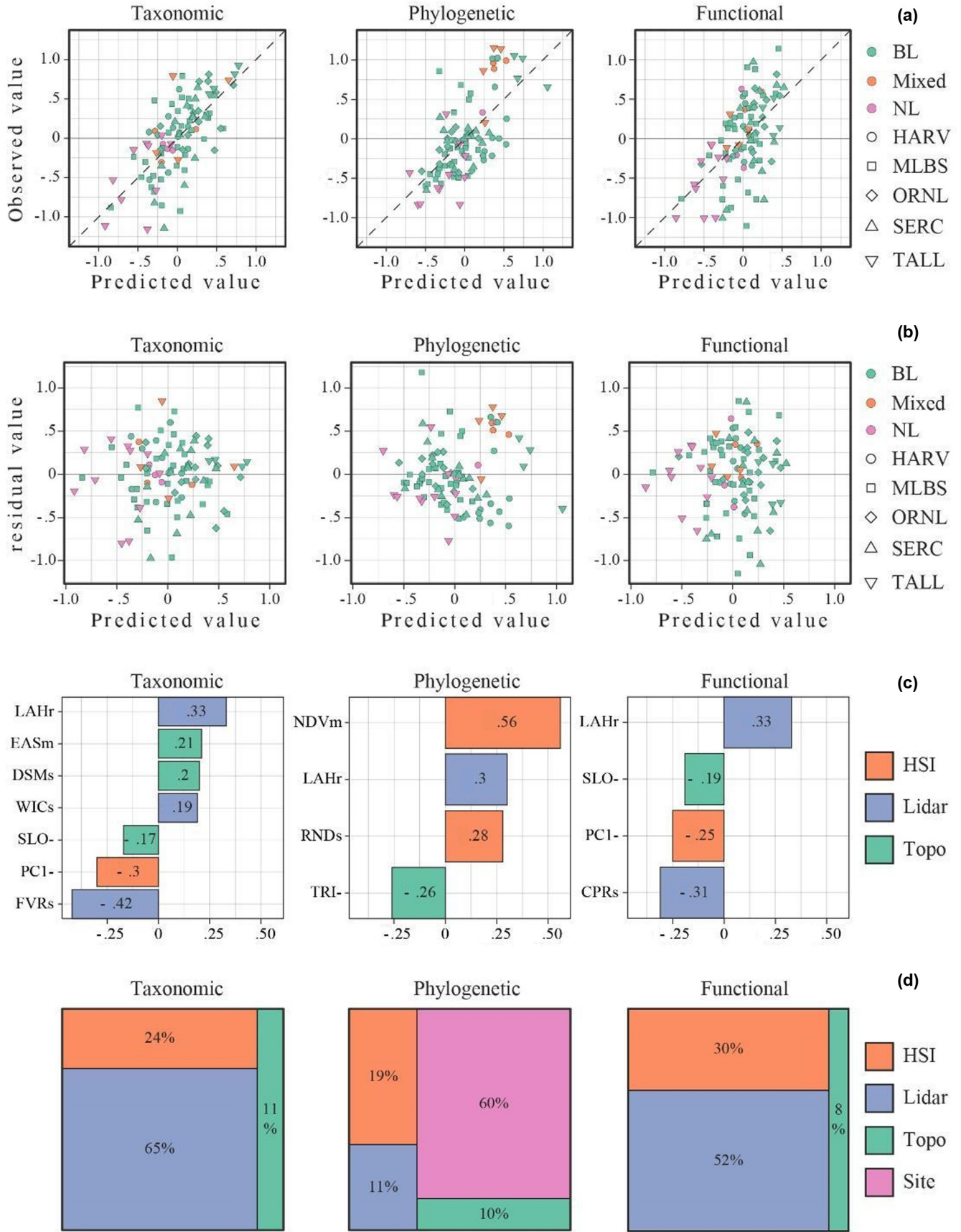
FIGURE 5 Results of final linear mixed effect (LME) models showing (a) observed versus predicted values, (b) residuals versus predicted values, (c) model coefficients, and (d) model percentage of R^2 of each sensor. Row (a) shows normalized observed versus predicted values from the final LME models, with the dotted line showing a 1:1 relationship. In rows (a) and (b), BL, NL, and Mixed refer to the percentage of functional types within each National Ecological Observatory Network (NEON) plot [i.e., BL = > 66% broadleaf species, NL = > 66% needleleaf species, Mixed = mixed broadleaf and needleleaf species (i.e., between 33 and 66% broadleaf)]. Site abbreviations found in Appendix A. Row (c) is labelled using metric abbreviations found in Table 1, with the last symbol signifying mean (m), minimum (−), range (r), or standard deviation (s) for each metric within the NEON field plot. In row (d), HSI refers to only hyperspectral derived remote sensing metrics, Lidar refers to lidar derived forest structure metrics, Topo refers to topographic metrics, and Site refers to random effects associated with broader site level differences

Moreover, within this joint analysis framework lidar-derived 3-D forest structure had the strongest relationship with taxonomic and functional biodiversity within the temperate forest biome (Figure 5c). This structure–function relationship has been reported in other temperate forest ecosystems (Gough et al., 2019; Hardiman et al., 2011, 2013), further demonstrating the importance of including structure, not just reflectance, in considerations of forest properties. This is also congruent with growing understanding of the role of canopy structural and environmental heterogeneity – features to which lidar is uniquely sensitive – in determining forest function (Bonan et al., 2021).

Site-level differences also had a large influence on our phylogenetic diversity model, contributing more than 35% to prediction of variance (70% overall, the strongest diversity prediction). Phylogenetic diversity in our study area was largely driven by whether a plot or site was dominated by broadleaf (angiosperm) or a mix of broadleaf and needleleaf (gymnosperm) trees. The importance of site to predicting phylogenetic diversity suggests that at this spatial scale and within eastern US temperate forests, phylogenetic diversity metrics may be driven by inter-site differences within forest regions related to the spatial distribution of plant functional types. And while environmental drivers may be implicated in the distributions of plant functional types, topography – the environmental driver that we studied – predicted < 20% of taxonomic diversity across sites. This suggests that any factor driving the site differences mostly varies on a scale larger than plots within sites, potentially including biogeographical factors such as the pool of available species in the region surrounding each site.

In contrast, site was rarely a significant predictor in our models of taxonomic and functional diversity. Thus, while our results show that we can explain a substantial fraction of field plot functional and taxonomic biodiversity across eastern US temperate forests (Table 1), the inclusion of finer-grained, within-site metrics related to soils, forest age, disturbance history, and climate could improve prediction. For instance, there are known differences in current and historic land use among and within NEON sites, which strongly influence vegetation (e.g., prescribed burns at TALL and historic land use at HARV; Foster, 1992) and patterns of diversity (Flatley et al., 2015; Paillet et al., 2010) and around the world there is increasing recognition of the role of humans in long-term ecosystem development (Ellis et al., 2021). At the scale of sites within a biome, the identity of stand-dominating species or taxa may also play a role in all components of diversity, particularly the

difference between broadleaf and needleleaf dominance, which dramatically alters structure and function (Atkins et al., 2018). Identifying forest composition and stand history with remote sensing data from characteristic structural patterns would complement the investigation of diversity and forest structure (e.g., Grabska et al., 2019; Sun et al., 2019); future diversity models will likely be improved by conditioning on this information. Finally, we note that because our study was confined to eastern US temperate forests with data collected only during peak greenness, isolating high NDVI pixels, lidar and hyperspectral variation was subtle; including phenological time series data could improve detection of relevant differences. More research will also be needed into how the presence of unhealthy, stressed and/or disturbed vegetation impacts these relationships.

Remote sensing of biodiversity studies can contain many sources of error and uncertainty related to sensors, resolution, and statistical methodologies. The remote sensing data used in this study were collected over multiple years using two different lidar sensors. Using lower pulse density lidar data also requires a coarser spatial resolution (i.e., 10 m × 10 m; Kamoske et al., 2019) than the hyperspectral data (i.e., 1 m × 1 m). While these data are derived at these nominal resolutions, they are ultimately aggregated to match the spatial grain of the field plots (i.e., 40 m × 40 m) and may be representing processes occurring at different scales. We also relied on hyperspectral diversity metrics, instead of hyperspectrally estimated trait maps. In the future, accurate trait maps could improve our models' performance, especially in predicting functional diversity; however, currently trait maps are not available for all sites (Wang et al., 2020) and where they have been challenged, some trait maps have been shown to differ substantially from field measurements (Pau et al., 2021). Estimating biodiversity metrics based on field data can also vary depending on methods; here we chose to use basal area weighted values, expecting that these would be more closely related to the metrics captured from above. As measures of biodiversity become a core component of environmental conservation, it is critical that researchers clarify exactly what they are measuring and mapping, both from the ground and from above.

With the increasing availability of airborne and spaceborne hyperspectral and lidar platforms like the NEON AOP, NASA Goddard's Lidar, Hyperspectral, & Thermal Imager (G-LiHT; Cook et al., 2013), the Global Ecosystem Dynamics Investigation (GEDI; Stavros et al., 2017), and the proposed Surface Biology and Geology Mission (SBG; Cawse-Nicholson et al., 2021) there is a unique opportunity to

ask and answer questions related to the spatial distribution of different dimensions of biodiversity not only within a given biome, but also across continents. While this study focuses on a single biome representing multiple forest types at the fine spatial grain of individual field plots, these findings can be applied to studies focused on continental scales. At continental scales, an important question will be whether universal models or ones conditioned within biomes will perform better and reveal more about biodiversity and forest structure. With an abundance of hyperspectral and lidar data being collected across a variety of biomes with new space and airborne remote sensing platforms, we have an opportunity to expand these methodologies to unlock important insights into how different dimensions of biodiversity vary and respond to global change. While more research is needed to assess these relationships across different ecoregions and at continental scales, the ever-increasing availability of hyperspectral and lidar data, in concert with targeted field campaigns, will provide new and exciting opportunities (Cavender-Bares et al., 2022).

5 | CONCLUSIONS

To facilitate the use of remote sensing for biodiversity monitoring, we present a reproducible methodology to calculate lidar, hyperspectral, and topographic derived metrics that are related to different dimensions of alpha diversity within the North American temperate forest biome. We show that a fusion of metrics derived from these different sensor types performs better at measuring biodiversity than each predictor type alone and that forest structure plays a significant role in all models. Moreover, our results suggest that while there are significant intra-site differences between our biodiversity variables due to differing local forest stand types (i.e., broadleaf and needleleaf), there are few inter-site differences between plots of the same stand type. Our results show that accurately mapping within-biome variation in biodiversity, and biodiversity change, from above will require a suite of active and passive remote sensing tools along with careful consideration of biogeographical differences within and among biomes.

DATA AVAILABILITY STATEMENT

Lidar and hyperspectral (HSI) data are available at: https://data.neonscience.org. R package to estimate structural traits from airborne lidar data is provided through our GitHub at: https://github.com/akamoske/canopyLazR. R package to pre-process HSI data is provided through our GitHub at: https://github.com/akamoske/hypRspec. R code to calculate hyperspectral metrics is provided through our GitHub at: https://github.com/akamoske/SpectralDiversity.

ORCID

Aaron G. Kamoske https://orcid.org/0000-0003-0222-4537
Quentin D. Read https://orcid.org/0000-0003-4315-5582
Phoebe L. Zarnetske https://orcid.org/0000-0001-6257-6951

REFERENCES

Asner, G. P., & Martin, R. E. (2016). Spectranomics: Emerging science and conservation opportunities at the interface of biodiversity and remote sensing. *Global Ecology and Conservation*, *8*, 212–219. https://doi.org/10.1016/j.gecco.2016.09.010

Atkins, J. W., Fahey, R. T., Hardiman, B. S., & Gough, C. M. (2018). Forest canopy structural complexity and light absorption relationships at the subcontinental scale. *Journal of Geophysical Research: Biogeosciences*, *123*(4), 1387–1405. https://doi.org/10.1002/2017JG004256

Auclair, A. N., & Cottam, G. (1971). Dynamics of Black Cherry (Prunus serotine Erhr.) in Southern Wisconsin Oak Forests. *Ecological Monographs*, *41*(2), 153–177.

Baiser, B., & Lockwood, J. L. (2011). The relationship between functional and taxonomic homogenization. *Global Ecology and Biogeography*, *20*, 134–144. https://doi.org/10.1111/j.1466-8238.2010.00583.x

Baiser, B., Olden, J. D., Record, S., Lockwood, J. L., & McKinney, M. L. (2012). Pattern and process of biotic homogenization in the New Pangaea. *Proceedings of the Royal Society B: Biological Sciences*, *279*(1748), 4772–4777. https://doi.org/10.1098/rspb.2012.1651

Barnett, D. T., Duffy, P. A., Schimel, D. S., Krauss, R. E., Irvine, K. M., Davis, F. W., Gross, J. E., Azuaje, E. I., Thorpe, A. S., Gudex-Cross, D., Patterson, M., McKay, J. M., McCorkel, J. T., & Meier, C. L. (2019). The terrestrial organism and biogeochemistry spatial sampling design for the National Ecological Observatory Network. *Ecosphere*, *10*(2), e02540. https://doi.org/10.1002/ecs2.2540

Bengtsson, J., Nilsson, S. G., Franc, A., & Menozzi, P. (2000). Biodiversity, disturbances, ecosystem function and management of European Forests. *Forest Ecology and Management*, *132*(1), 39–50. https://doi.org/10.1016/S0378-1127(00)00378-9

Bergen, K. M., Goetz, S. J., Dubayah, R. O., Henebry, G. M., Hunsaker, C. T., Imhoff, M. L., Nelson, R. F., Parker, G. G., & Radeloff, V. C. (2009). Remote sensing of vegetation 3-D structure for biodiversity and habitat: Review and implications for lidar and radar spaceborne missions. *Journal of Geophysical Research*, *114*, 1–13. https://doi.org/10.1029/2008JG000883

Bonan, G. B. (2008). Forests and climate change: Forcings, feedbacks, and the climate benefits of forests. *Science*, *320*(5882), 1444–1449. https://doi.org/10.1126/science.1155121

Bonan, G. B., Patton, E. G., Finnigan, J. J., Baldocchi, D. D., & Harman, I. N. (2021). Moving beyond the incorrect but useful paradigm: Reevaluating big-leaf and multilayer plant canopies to model biosphere-atmosphere fluxes–a review. *Agricultural and Forest Meteorology*, *306*, 108435. https://doi.org/10.1016/j.agrformet.2021.108435

Boyce, M. S. (2006). Scale for resource selection functions. *Diversity and Distributions*, *12*, 269–276. https://doi.org/10.1111/j.1366-9516.2006.00243.x

Brook, B. W., Sodhi, N. S., & Bradshaw, C. J. A. (2008). Synergies among extinction drivers under global change. *Trends in Ecology & Evolution*, *23*, 453–460. https://doi.org/10.1016/j.tree.2008.03.011

Bunker, D. E., DeClerck, F., Bradford, J. C., Colwell, R. K., Perfecto, I., Phillips, O. L., Sankaran, M., & Naeem, S. (2005). Species loss and aboveground carbon storage in a tropical forest. *Science*, *310*, 1029–1031. https://doi.org/10.1126/science.1117682

Burnham, K. P., Anderson, D. R., & Huyvaert, K. P. (2011). AIC model selection and multimodel inference in behavioral ecology: Some background, observations, and comparisons. *Behavioral Ecology and Sociobiology*, *65*, 23–35. https://doi.org/10.1007/s00265-010-1029-6

Bush, A., Sollmann, R., Wilting, A., Bohmann, K., Cole, B., Balzter, H., Martius, C., Zlinszky, A., Calvignac-Spencer, S., Cobbold, C. A., Dawson, T. P., Emerson, B. C., Ferrier, S., Gilbert, M. T. P., Herold, M., Jones, L., Leendertz, F. H., Matthews, L., Millington, J. D. A., … Yu, D. W. (2017). Connecting earth observation to high-throughput biodiversity data. *Nature Ecology & Evolution*, *1*, 1–9. https://doi.org/10.1038/s41559-017-0176

Cardinale, B. J., Duffy, J. E., Gonzalez, A., Hooper, D. U., Perrings, C., Venail, P., Narwani, A., Mace, G. M., Tilman, D., Wardle, D. A., Kinzig, A. P., Daily, G. C., Loreau, M., Grace, J. B., Larigauderie, A., Srivastava, D. S., & Naeem, S. (2012). Biodiversity loss and its impact on humanity. *Nature*, *486*, 59–67. https://doi.org/10.1038/nature11148

Cavender-Bares, J., Gamon, J. A., Hobbie, S. E., Madritch, M. D., Meireles, J. E., Schweiger, A. K., & Townsend, P. A. (2017). Harnessing plant spectra to integrate the biodiversity sciences across biological and spatial scales. *American Journal of Botany*, *104*(7), 966–969. https://doi.org/10.3732/ajb.1700061

Cavender-Bares, J., Kozak, K. H., Fine, P. V., & Kembel, S. W. (2009). The merging of community ecology and phylogenetic biology. *Ecology Letters*, *12*, 693–715. https://doi.org/10.1111/j.1461-0248.2009.01314.x

Cavender-Bares, J., Meireles, J. E., Couture, J. J., Kaproth, M. A., Kingdon, C. C., Singh, A., Serbin, S. P., Center, A., Zuniga, E., Pilza, G., & Townsend, P. A. (2016). Associations of leaf spectra with genetic and phylogenetic variation in oaks: prospects for remote detection of biodiversity. *Remote Sensing*, *8*(221), 1–17. https://doi.org/10.3390/rs8030221

Cavender-Bares, J., Schneider, F. D., Santos, M. J., Armstrong, A., Carnaval, A., Dahlin, K. M., Fatoyinbo, L., Hurtt, G. C., Schimel, D., Townsend, P. A., Ustin, S. L., Wang, Z., & Wilson, A. M. (2022). Integrating remote sensing with ecology and evolution to advance biodiversity conservation. *Nature Ecology & Evolution*. https://doi.org/10.1038/s41559-022-01702-5

Cawse-Nicholson, K., Townsend, P. A., Schimel, D., Assiri, A. M., Blake, P. L., Buongiorno, M. F., Campbell, P., Carmon, N., Casey, K. A., Correa-Pabón, R. E., Dahlin, K. M., Dashti, H., Dennison, P. E., Dierssen, H., Erickson, A., Fisher, J. B., Frouin, R., Gatebe, C. K., Gholizadeh, H., … Zhang, Q. (2021). NASA's surface biology and geology designated observable: A perspective on surface imaging algorithms. *Remote Sensing of Environment*, *257*, 112349. https://doi.org/10.1016/j.rse.2021.112349

Chase, J. (2010). Stochastic community assembly causes high biodiversity in more productive environments. *Science*, *328*(5984), 1388–1391.

Chen, J. M., & Black, T. A. (1992). Defining leaf area index for non-flat leaves. *Plant, Cell and Environment*, *15*, 421–429.

Colgan, M. S., Baldeck, C. A., Baptiste Féret, J., & Asner, G. P. (2012). Mapping savanna tree species at ecosystem scales using support vector machine classification and BRDF correction on airborne hyperspectral and LiDAR data. *Remote Sensing*, *4*, 3462–3480. https://doi.org/10.3390/rs4113462

Collings, S., Caccetta, P., Campbell, N., & Wu, X. (2010). Techniques for BRDF correction of hyperspectral mosaics. *IEEE Transactions on Geoscience and Remote Sensing*, *48*, 3733–3746. https://doi.org/10.1109/TGRS.2010.2048574

Cook, B., Corp, L., Nelson, R., Middleton, E., Morton, D., McCorkel, J., Masek, J., Ranson, K., Ly, V., & Montesano, P. (2013). NASA Goddard's LiDAR, hyperspectral and thermal (G-LiHT) airborne imager. *Remote Sensing*, *5*, 4045–4066. https://doi.org/10.3390/rs5084045

Cooper, W. J., McShea, W. J., Luther, D. A., & Forrester, T. (2019). Incorporating local habitat heterogeneity and productivity measures when modelling vertebrate richness. *Environmental Conservation*, *1*, 8. https://doi.org/10.1017/S0376892919000328

Cosovic, M., Bugalho, M. N., Thom, D., & Borges, J. G. (2020). Stand structural characteristics are the most practical biodiversity indicators for forest management planning Europe. *Forests*, *11*(343), 1–24.

Dahlin, K. M. (2016). Spectral diversity area relationships for assessing biodiversity in a wildland-agriculture matrix. *Ecological Applications*, *26*(8), 2758–2768.

Dahlin, K. M., Asner, G. P., & Field, C. B. (2012). Environmental filtering and land-use history drive patterns in biomass accumulation in a mediterranean-type landscape. *Ecological Applications*, *22*(1), 104–118. https://doi.org/10.1890/11-1401.1

Dahlin, K. M., Asner, G. P., & Field, C. B. (2014). Linking vegetation patterns to environmental gradients and human impacts in a mediterranean-type island ecosystem. *Landscape Ecology*, *29*, 1571–1585. https://doi.org/10.1007/s10980-014-0076-1

Dalponte, M., Bruzzone, L., & Gianelle, D. (2008). Fusion of hyperspectral and lidar remote sensing data for classification of complex forest areas. *IEEE Transactions on Geoscience and Remote Sensing*, *46*(5), 1416–1427. https://doi.org/10.1109/TGRS.2008.916480

Dambrine, E., Dupouey, J. L., Laut, L., Humbert, L., Thinon, M., Beaufils, T., & Richard, H. (2007). Present forest biodiversity patterns in France related to former roman agriculture. *Ecology*, *88*(6), 1430–1439. https://doi.org/10.1890/05-1314

Dupouey, J. L., Dambrine, E., Laffite, J. D., & Moares, C. (2002). Irreversible impact of past land use on forest soils and biodiversity. *Ecology*, *83*(11), 2978–2984.

Duro, D. C., Coops, N. C., Wulder, M. A., & Han, T. (2007). Development of a large area biodiversity monitoring system driven by remote sensing. *Progress in Physical Geography*, *31*(3), 235–260. https://doi.org/10.1177/0309133307079054

Dyer, J. (2006). Revisting the deciduous forests of Eastern North America. *BioScience*, *56*(4), 341–352.

Ellis, E., Gauthier, N., Goldewijk, K., Bird, R. B., Boivin, N., Díaz, S., Fuller, D. Q., Gill, J. L., Kaplan, J. O., Kingston, N., & Locke, H. (2021). People have shaped most of terrestrial nature for at least 12,000 years. *Proceedings of the National Academy of Sciences of the United States of America*, *118*(17), e2023483118.

Feret, J. B., & Asner, G. P. (2014). Mapping tropical forest canopy diversity using high-fidelity imaging spectroscopy. *Ecological Applications*, *24*(6), 1289–1296. https://doi.org/10.1890/13-1824.1

Flatley, W. T., Lafon, C. W., Grissino-Mayer, H. D., & LaForest, L. B. (2015). Changing fire regimes and old-growth forest succession along a topographic gradient in the Great Smoky Mountains. *Forest Ecology and Management*, *350*, 96–106. https://doi.org/10.1016/j.foreco.2015.04.024

Flynn, D. F. B., Mirotchnick, N., Jain, M., Palmer, M. I., & Naeem, S. (2011). Functional and phylogenetic diversity as predictors of biodiversity–ecosystem-function relationships. *Ecology*, *92*, 1573–1581. https://doi.org/10.1890/10-1245.1

Foster, D. R. (1992). Land-use history (1730–1990) and vegetation dynamics in Central New England, USA. *Ecology*, 80(4), 753–771. https://doi.org/10.2307/2260864

Gamon, J. A., Penuelas, J., & Field, C. B. (1992). A narrow-waveband spectral index that tracks diurnal changes in photosynthetic efficiency. *Remote Sensing of Environment*, 41, 35–44.

Gaston, K. J. (2000). Global patterns in biodiversity. *Nature*, 405, 220–227. https://doi.org/10.1038/35012228

Gelman, A. (2008). Scaling regression inputs by dividing by two standard deviations. *Statistics in Medicine*, 27, 2865–2873. https://doi.org/10.1002/sim.3107

Gholizadeh, H., Gamon, J. A., Townsend, P. A., Zygielbaum, A. I., Helzer, C. J., Hmimina, G. Y., Yu, R., Moore, R. M., Schweiger, A. K., & Cavender-Bares, J. (2019). Detecting prairie biodiversity with airborne remote sensing. *Remote Sensing of Environment*, 221, 38–49. https://doi.org/10.1016/j.rse.2018.10.037

Gholizadeh, H., Gamon, J. A., Zygielbaum, A. I., Wang, R., Schweiger, A. K., & Cavender-Bares, J. (2018). Remote sensing of biodiversity: Soil correction and data dimension reduction methods improve assessment of a-diversity (species richness) in prairie ecosystems. *Remote Sensing of Environment*, 206, 240–253.

Gitelson, A., & Merzlyak, M. (1994). Spectral reflectance changes associated with autumn senescence of Aesculus Hippocastanum L. and Acer Platanoides L. Leaves. *Journal of Plant Physiology*, 143, 286–292.

Goolsby, E. W., Ane, C., & Bruggeman, J. (2017). Rphylopars: Fast multivariate phylogenetic comparative methods for missing data and within-species variation. *Methods in Ecology & Evolution*, 8, 22–27. https://doi.org/10.1111/2041-210X.12612

Gotelli, N., & Ellison, A. M. (2013). *A primer of ecological statistics*. Sinauer Associates Inc.

Gough, C. M., Atkins, J. W., Fahey, R. T., & Hardiman, B. S. (2019). High rates of primary production in structurally complex forests. *Ecology*, 100. https://doi.org/10.1002/ecy.2864

Gough, C. M., Atkins, J., Fahey, R., Hardiman, B., & LaRue, E. (2020). Community and structural constrains on the complexity of eastern North American forests. *Global Ecology and Biogeography*, 29(12), 2107–2118.

Grabska, E., Hostert, P., Pflugmacher, D., & Ostapowicz, K. (2019). Forest stand species mapping using the Sentinel-2 time series. *Remote Sensing*, 11(10), 1197. https://doi.org/10.3390/rs11101197

Hardiman, B. S., Bohrer, G., Gough, C. M., Vogel, C. S., Curtis, P. S., Vogel, S., Curtis, S., & Hardiman, S. (2011). The role of canopy structural complexity in wood net primary production of a maturing northern deciduous forest. *Ecology*, 92, 1818–1827. https://doi.org/10.1890/10-2192.1

Hardiman, B. S., Gough, C. M., Halperin, A., Hofmeister, K. L., Nave, L. E., Bohrer, G., & Curtis, P. S. (2013). Maintaining high rates of carbon storage in old forests: A mechanism linking canopy structure to forest function. *Forest Ecology and Management*, 298, 111–119. https://doi.org/10.1016/j.foreco.2013.02.031

He, K. S., Bradley, B. A., Cord, A. F., Rocchini, D., Tuanmu, M.-N., Schmidtlein, S., Turner, W., Wegmann, M., & Pettorelli, N. (2015). Will remote sensing shape the next generation of species distribution models? *Remote Sensing in Ecology and Conservation*, 1, 4–18. https://doi.org/10.1002/rse2.7

Hooper, D. U., Adair, E. C., Cardinale, B. J., Byrnes, J. E. K., Hungate, B. A., Matulich, K. L., Gonzalez, A., Duffy, J. E., Gamfeldt, L., & O'Connor, M. I. (2012). A global synthesis reveals biodiversity loss as a major driver of ecosystem change. *Nature*, 486, 105–108. https://doi.org/10.1038/nature11118

Isbell, F., Craven, D., Connolly, J., Loreau, M., Schmid, B., Beierkuhnlein, C., Bezemer, T. M., Bonin, C., Bruelheide, H., De Luca, E., Ebeling, A., Griffin, J. N., Guo, Q., Hautier, Y., Hector, A., Jentsch, A., Kreyling, J., Lanta, V., Manning, P., … Eisenhauer, N. (2015). Biodiversity

increases the resistance of ecosystem productivity to climate extremes. *Nature*, 526, 574–577. https://doi.org/10.1038/nature15374

Jetz, W., McGeoch, M. A., Guralnick, R., Ferrier, S., Beck, J., Costello, M. J., Fernandez, M., Geller, G. N., Keil, P., Merow, C., Meyer, C., Muller-Karger, F. E., Pereira, H. M., Regan, E. C., Schmeller, D. S., & Turak, E. (2019). Essential biodiversity variables for mapping and monitoring species populations. *Nature Ecology & Evolution*, 3, 539–551. https://doi.org/10.1038/s41559-019-0826-1

Jost, L. (2006). Entropy and diversity. *Oikos*, 113(2), 363–375.

Jost, L. (2007). Partitioning diversity into independent alpha and beta components. *Ecology*, 88(10), 2427–2439. https://doi.org/10.1890/06-1736.1

Kamoske, A. G., Dahlin, K. M., Serbin, S. P., & Stark, S. C. (2020). Leaf traits and canopy structure together explain canopy functional diversity: An airborne remote sensing approach. *Ecological Applications*, 31(2), e02230. https://doi.org/10.1002/eap.2230

Kamoske, A. G., Dahlin, K. M., Stark, S. C., & Serbin, S. P. (2019). Leaf area density from airborne LiDAR: Comparing sensors and resolutions in a temperate broadleaf forest ecosystem. *Forest Ecology and Management*, 433, 364–375. https://doi.org/10.1016/j.foreco.2018.11.017

Kampe, T. U., Johnson, B. R., Kuester, M., & Keller, M. (2010). NEON: The first continental-scale ecological observatory with airborne remote sensing of vegetation canopy biochemistry and structure. *Journal of Applied Remote Sensing*, 4, 043510. https://doi.org/10.1117/1.3361375

Kattge, J., Boenisch, G., Diaz, S., Lavorel, S., Prentice, I. C., Leadley, P., Tautenhahn, S., Werner, G. D., Aakala, T., Abedi, M., & Acosta, A. T. (2020). TRY plant trait database - enhance coverage and open access. *Global Change Biology*, 26, 119–188.

Keddy, P. A. (1992). Assembly and response rules: Two goals for predictive community ecology. *Journal of Vegetation Science*, 3(2), 157–164. https://doi.org/10.2307/3235676

Korhonen, L., Korpela, I., Heiskanen, J., & Maltamo, M. (2011). Airborne discrete-return LIDAR data in the estimation of vertical canopy cover, angular canopy closure and leaf area index. *Remote Sensing of Environment*, 115, 1065–1080.

Kreft, H., & Jetz, W. (2007). Global patterns and determinants of vascular plant diversity. *Proceedings of the National Academy of Sciences of the United States of America*, 104(14), 5925–5930. https://doi.org/10.1073/pnas.0608361104

Laliberté, E., Schweiger, A. K., & Legendre, P. (2020). Partitioning plant spectral diversity into alpha and beta components. *Ecology Letters*, 23, 370–380. https://doi.org/10.1111/ele.13429

LaRue, E. A., Hardiman, B. S., Elliot, J. M., & Fei, S. (2019). Structural diversity as a predictor of ecosystem function. *Environmental Research Letters*, 14(11), 114011. https://doi.org/10.1088/1748-9326/ab49bb

Leblanc, S. G., Chen, J. M., Fernandes, R., Deering, D. W., & Conley, A. (2005). Methodology comparison for canopy structure parameters extraction from digital hemispherical photography in boreal forests. *Agricultural and Forest Meteorology*, 129, 187–207. https://doi.org/10.1016/j.agrformet.2004.09.006

Lefsky, M. A., Cohen, W. B., Acker, S. A., Parker, G. G., Spies, T. A., & Harding, D. (1999). Lidar remote sensing of the canopy structure and biophysical properties of douglas-fir western hemlock forests. *Remote Sensing of Environment*, 70, 339–361.

Leutner, B. F., Reineking, B., Muller, J., Bachmann, M., Beierkuhnlein, C., Dech, S., & Wegmann, M. (2012). Modelling forest α-diversity and floristic composition – on the added value of LiDAR plus hyperspectral remote sensing. *Remote Sensing*, 4, 2818–2845. https://doi.org/10.3390/rs4092818

Li, D., Olden, J. D., Lockwood, J. L., Record, S., McKinney, M. L., & Baiser, B. (2020). Changes in taxonomic and phylogenetic diversity in the Anthropocene. *Proceedings of the Royal Society B:*

Biological Sciences, *287*, 20200777. https://doi.org/10.1098/rspb.2020.0777

Lomolino, M. V., Riddle, B. R., Whittaker, R. J., & Brown, J. H. (2010). *Biogeography* (4th ed.). Sinauer.

MacArthur, R. H., & Horn, H. S. (1969). Foliage profile by vertical measurements. *Ecology*, *50*, 802–804. https://doi.org/10.2307/1933693

Mascaro, J., Asner, G. P., Muller-Landau, H. C., Van Breugel, M., Hall, J., & Dahlin, K. (2011). Controls over aboveground forest carbon density on Barro Colorado Island, Panama. *Biogeosciences*, *8*, 1615–1629. https://doi.org/10.5194/bg-8-1615-2011

Massante, J. C., Götzenberger, L., Takkis, K., Hallikma, T., Kaasik, A., Laanisto, L., Hutchings, M. J., & Gerhold, P. (2019). Contrasting latitudinal patterns in phylogenetic diversity between woody and herbaceous communities. *Nature*, *9*, 6443. https://doi.org/10.1038/s41598-019-42827-1

Meireles, J. E., Cavender-Bares, J., Townsend, P. A., Ustin, S., Gamon, J. A., Schweiger, A. K., Schaepman, M. E., Asner, G. P., Martin, R. E., Singh, A., & Schrodt, F. (2020). Leaf reflectance spectra capture the evolution of seed plants. *New Phytologist*, *228*, 485–493.

Miller, J. (1967). A formula for average foliage density. *Australian Journal of Botany*, *15*, 141.

Morlon, H., Schwilk, D., Bryant, J., Marquet, P., Rebelo, A., Tauss, C., Bohanna, B., & Green, J. (2010). Spatial patterns of phylogenetic diversity. *Ecology Letters*, *14*(2), 141–149. https://doi.org/10.1111/j.1461-0248.2010.01563.x

Merton, R. N., & Huntington, J. F. (1999). Early simulation results of the ARIES-1 satellite sensor for multi-temporal vegetation research derived from AVIRIS. Proceedings of the Eighth Annual JPL Airborne Earth Science Workshop. NASA, Jet Propulsion Laboratory, Pasadena, California, USA. 8-14 February 1999.

National Ecological Observatory Network. (2020). Data Products NEON.DP1.10098.001. Battelle. Provisional data downloaded from http://data.neonscience.org on 04 April 2020

Olden, J. D., & Rooney, T. P. (2006). On defining and quantifying biotic homogenization. *Global Ecology and Biogeography*, *15*, 113–120. https://doi.org/10.1111/j.1466-822X.2006.00214.x

Ollinger, S. V. (2011). Sources of variability in canopy reflectance and the convergent properties of plants. *New Phytologist*, *189*(2), 375–394.

Oldeland, J., Wesuls, D., Rocchini, D., Schmidt, M., & Jürgens, N. (2010). Does using species abundance data improve estimates of species diversity from remotely sensed spectral heterogeneity? *Ecological Indicators*, *10*, 390–396.

Ozanne, C. M. P., Anhug, D., Boulter, S. L., Keller, M., Kitching, R. L., Korner, C., Meinzer, F. C., Mitchell, A. W., Nakashizuka, T., Silva Dias, P. L., Stork, N. E., Wright, S. J., & Yoshimura, M. (2003). Biodiversity meets the atmosphere: A global view of forest canopies. *Science*, *301*, 183–186. https://doi.org/10.1126/science.1084507

Paillet, Y., Bergès, L., Hjältén, J., Ódor, P., Avon, C., Bernhardt-römermann, M., Bijlsma, R.-J., De Bruyn, L., Fuhr, M., Grandin, U., Kanka, R., Lundin, L., Luque, S., Magura, T., Matesanz, S., Mészáros, I., Sebastià, M.-T., Schmidt, W., Standovár, T., … Virtanen, R. (2010). Biodiversity differences between managed and unmanaged forests: Meta-analysis of species richness in Europe. *Conservation Biology*, *24*(1), 101–112. https://doi.org/10.1111/j.1523-1739.2009.01399.x

Parmesan, C., & Yohe, G. (2003). A globally coherent fingerprint of climate change impacts across natural systems. *Nature*, *421*, 37–42. https://doi.org/10.1038/nature01286

Pau, S., Nippert, J. B., Slapikas, R., Griffith, D., Bachle, S., Helliker, B. R., O'Connor, R. C., Riley, W. J., Still, C. J., & Zaricor, M. (2021). Poor relationships between NEON airborne observation platform data and field-based vegetation traits at a mesic grassland. *Ecology*, e03590. https://doi.org/10.1002/ecy.3590

Petchy, O., & Gaston, K. (2006). Functional diversity: Back to basics and looking forward. *Ecology Letters*, *9*(6), 741–758. https://doi.org/10.1111/j.1461-0248.2006.00924.x

Pettorelli, N., Safi, K., & Turner, W. (2014). Satellite remote sensing, biodiversity research and conservation of the future. *Philosophical Transactions of the Royal Society B: Biological Sciences*, *369*, 20130190.

Pinheiro, J. C., & Bates, D. M. (2000). *Mixed-effects models in S and S-PLUS*. Springer.

Potter, K. M., & Koch, F. H. (2014). Patterns of forest phylogenetic community structure across the United States and their possible forest health implications. *Forest Science*, *60*, 851–861. https://doi.org/10.5849/forsci.13-115

Potter, K. M., & Woodall, C. W. (2012). Trends over time in tree and seedling phylogenetic diversity indicate regional differences in forest biodiversity change. *Ecological Applications*, *22*, 517–531. https://doi.org/10.1890/10-2137.1

QGIS.org (2022). QGIS Geographic Information System. QGIS Association. http://www.qgis.org

R Core Team (2021). *R: A language and environment for statistical computing*. R Foundation for Statistical Computing. https://www.R-project.org/

Read, Q. D., Zarnetske, P. L., Record, S., Dahlin, K. M., Costanza, J. K., Finley, A. O., Gaddis, K. D., Grady, J. M., Hobi, M. L., Latimer, A. M., Malone, S. L., Ollinger, S. V., Pau, S., & Wilson, A. M. (2019). Beyond counts and averages: Relating geodiversity to dimensions of biodiversity. *Global Ecology and Biogeography*, *00*, 1–15.

Record, S., Dahlin, K. M., Zarnetske, P. L., Read, Q. D., Malone, S. L., Gaddis, K. D., Grady, J. M., Costanza, J., Hobi, M. L., Latimer, A. M., & Pau, S. (2020). Remote sensing of geodiversity as a link to biodiversity. In J. Cavender-Bares, J. A. Gamon, & P. A. Townsend (Eds.), *Remote sensing of plant biodiversity*. Springer Open Press.

Reich, P. B., Bakken, P., Carlson, D., Frelich, L. E., Friedman, S. K., & Grigal, D. F. (2001). Influence of logging, fire, and forest type on biodiversity and productivity in Southern Boreal Forests. *Ecology*, *82*(10), 2731–2748.

Richardson, J. J., Moskal, L. M., & Kim, S. H. (2009). Modeling approaches to estimate effective leaf area index from aerial discrete-return LIDAR. *Agricultural and Forest Meteorology*, *149*, 1152–1160. https://doi.org/10.1016/j.agrformet.2009.02.007

Roscher, C., Schumacher, J., Gubsch, M., Lipowsky, A., Weigelt, A., Buchmann, N., Schmid, B., & Schulze, E. (2012). Using plant functional traits to explain diversity-productivity relationships. *PLoS One*, *7*(5), e36760. https://doi.org/10.1371/journal.pone.0036760

Rouse, J. W., Haas, R. H., Schell, J. A., & Deering, D. W. (1974). Monitoring vegetation systems in the great plains with ERTAS. In S. C. Freden, E. P. Mercanti, & M. Becker (Eds.), *Third Earth Resources Technology Satellite-1 Symposium. Volume 1: Technical Presentations*, NASA SP-351 (Vol. *1*, pp. 309–317). NASA.

Sabol, J., Patočka, Z., & Mikita, T. (2014). Usage of lidar data for leaf area index estimation. *GeoScience Engineering*, *60*, 10–18. https://doi.org/10.2478/gse-2014-0013

Säfken, B., Rügamer, D., Kneib, T., & Greven, S. (2021). Conditional model selection in mixed-effects models with cAIC4. *Journal of Statistical Software*, *99*(8), 1–30. https://doi.org/10.18637/jss.v099.i08

Schlapfer, D., Richter, R., & Feingersh, T. (2015). Operational BRDF effects correction for wide-field-of-view optical scanners (BREFCOR). *IEEE Transactions on Geoscience and Remote Sensing*, *53*, 1855–1864. https://doi.org/10.1109/TGRS.2014.2349946

Schmitt, S., Marechaux, I., Chave, J., Fischer, F., Piponiot, C., Traissac, S., & Herault, B. (2019). Functional diversity improves tropical forest resilience: Insights from a long-term virtual experiment. *Journal of Ecology*, *108*(3), 831–843. https://doi.org/10.1111/1365-2745.13320

Shi, Y., Wang, T., Skidmore, A. K., & Heurich, M. (2018). Important LiDAR metrics for discriminating forest tree species in Central Europe. *ISPRS Journal of Photogrammetry and Remote Sensing*, *137*, 163–174.

Shao, G., Stark, S. C., de Almeida, D. R. A., & Smith, M. N. (2019). Towards high throughput assessment of canopy dynamics: The estimation of leaf area structure in Amazonian forests with multitemporal multi-sensor airborne lidar. *Remote Sensing of Environment*, *221*, 1–13. https://doi.org/10.1016/j.rse.2018.10.035

Simonson, W. D., Allen, H. D., & Coomes, D. A. (2012). Use of an airborne lidar system to model plant species composition and diversity of Mediterranean Oak Forests. *Conservation Biology*, *26*(5), 840–850. https://doi.org/10.1111/j.1523-1739.2012.01869.x

Skidmore, A. K., Coops, N. C., Neinavaz, E., Ali, A., Schaepman, M. E., Paganini, M., Kissling, W. D., Vihervaara, P., Darvishzadeh, R., Feilhauer, H., & Fernandez, M. (2021). Priority list of biodiversity metrics to observe from space. *Nature Ecology & Evolution*, *5*(7), 896–906.

Soenen, S. A., Peddle, D. R., & Coburn, C. A. (2005). SCS+C: A modified Sun-canopy-sensor topographic correction in forested terrain. *IEEE Transactions on Geoscience and Remote Sensing*, *43*, 2148–2159. https://doi.org/10.1109/TGRS.2005.852480

Solberg, S., Næsset, E., Hanssen, K. H., & Christiansen, E. (2006). Mapping defoliation during a severe insect attack on Scots pine using airborne laser scanning. *Remote Sensing of Environment*, *102*, 364–376. https://doi.org/10.1016/j.rse.2006.03.001

Spellerberg, I. F., & Fedor, P. J. (2003). A tribute to Claude Shannon (1916–2001) and a plea for more rigorous use of species richness, species diversity and the 'Shannon–Wiener' Index. *Global Ecology and Biogeography*, *12*(3), 177–179. https://doi.org/10.1046/j.1466-822X.2003.00015.x

Srivastava, D. S., Cadotte, M. W., MacDonald, A. A. M., Marushia, R. G., & Mirotchnick, N. (2012). Phylogenetic diversity and the functioning of ecosystems. *Ecology Letters*, *15*, 637–648. https://doi.org/10.1111/j.1461-0248.2012.01795.x

Stark, S. C., Enquist, B. J., Saleska, S. R., Leitold, V., Schietti, J., Longo, M., Alves, L. F., Camargo, P. B., & Oliveira, R. C. (2015). Linking canopy leaf area and light environments with tree size distributions to explain Amazon forest demography. *Ecology Letters*, *18*, 636–645. https://doi.org/10.1111/ele.12440

Stark, S. C., Leitold, V., Wu, J. L., Hunter, M. O., de Castilho, C. V., Costa, F. R. C., Mcmahon, S. M., Parker, G. G., Shimabukuro, M. T., Lefsky, M. A., Keller, M., Alves, L. F., Schietti, J., Shimabukuro, Y. E., Brandão, D. O., Woodcock, T. K., Higuchi, N., de Camargo, P. B., de Oliveira, R. C., & Saleska, S. R. (2012). Amazon forest carbon dynamics predicted by profiles of canopy leaf area and light environment. *Ecology Letters*, *15*, 1406–1414. https://doi.org/10.1111/j.1461-0248.2012.01864.x

Stavros, E. N., Schimel, D., Pavlick, R., Serbin, S., Swann, A., Duncanson, L., Fisher, J. B., Fassnacht, F., Ustin, S., Dubayah, R., Schwigher, A., & Wennberg, P. (2017). ISS observations offer insights into plant function. *Nature Ecology and Evolution*, *1*, 1–4. https://doi.org/10.1038/s41559-017-0194

Stevens, J. T., Kling, M. W., Schwilk, D. W., Varner, J. M., & Kane, J. M. (2020). Biogeography of fire regimes in western U.S. conifer forests: A trait-based approach. *Global Ecology and Biogeography*, *29*(5), 944–955. https://doi.org/10.1111/geb.13079

Sumida, A., Nakai, T., Yamada, M., Ono, K., Uemura, S., & Hara, T. (2009). Ground-based estimation of leaf area index and vertical distribution of leaf area density in a betula ermanii forest. *Silva Fennica*, *43*, 799–816. https://doi.org/10.14214/sf.174

Sun, C., Cao, S., & Sanchez-Azofeifa, G. A. (2019). Mapping tropical dry forest age using airborne waveform LiDAR and hyperspectral metrics. *International Journal of Applied Earth Observation and Geoinformation*, *83*, 101908. https://doi.org/10.1016/j.jag.2019.101908

Swenson, N. G., Enquist, B. J., Pither, J., Kerkhoff, A. J., Boyle, B., Weiser, M. D., Elser, J. J., Fagan, W. F., Forero-Montaña, J., Fyllas, N., Kraft, N. J. B., Lake, J. K., Moles, A. T., Patiño, S., Phillips, O. L., Price, C. A., Reich, P. B., Quesada, C. A., Stegen, J. C., ... Nolting, K. M. (2011). The biogeography and filtering of woody plant functional diversity in North and South America. *Global Ecology and Biogeography*, *21*(8), 798–808. https://doi.org/10.1111/j.1466-8238.2011.00727.x

Tews, J., Brose, U., Grimm, V., Tielbörger, K., Wichmann, M. C., Schwager, M., & Jeltsch, F. (2004). Animal species diversity driven by habitat heterogeneity/ diversity: The importance of keystone structures. *Journal of Biogeography*, *31*, 79–92. https://doi.org/10.1046/j.0305-0270.2003.00994.x

Thorpe, A. S., Barnett, D. T., Elmendorf, S. C., Hinckley, E. S., Hoekman, D., Jones, K. D., LeVan, K. E., Meier, C. L., Stanish, L. F., & Thibault, K. M. (2016). Introduction to the sampling designs of the National Ecological Observatory Network Terrestrial Observation System. *Ecosphere*, *7*(12), e01627.

Turner, W., Spector, S., Gardiner, N., Fladeland, M., Sterling, E., & Steininger, M. (2003). Remote sensing for biodiversity science and conservation. *Trends in Ecology & Evolution*, *18*, 306–314. https://doi.org/10.1016/S0169-5347(03)00070-3

Urban, M. C. (2015). Accelerating extinction risk from climate change. *Science*, *348*, 571–573. https://doi.org/10.1126/science.aaa4984

Venables, W. N., & Ripley, B. D. (2002). *Modern applied statistics with S*. Stanford University.

Wang, R., & Gamon, J. A. (2019). Remote sensing of terrestrial plant biodiversity. *Remote Sensing of Environment*, *231*, 211–218. https://doi.org/10.1016/j.rse.2019.111218

Wang, R., Gamon, J. A., Cavender-Bares, J., Townsend, P. A., & Zygielbaum, A. I. (2018). The spatial sensitivity of the spectral diversity-biodiversity relationship: An experimental test in a prairie grassland. *Ecological Applications*, *28*, 541–556. https://doi.org/10.1002/eap.1669

Wang, Z., Chlus, A., Geygan, R., Ye, Z., Zheng, T., Singh, A., Couture, J. J., Cavender-Bares, J., Kruger, E. L., & Townsend, P. A. (2020). Foliar functional traits from imaging spectroscopy across biomes in eastern North America. *New Phytologist*, *228*(2), 494–511. https://doi.org/10.1111/nph.16711

Wanner, W., Li, X., & Strahler, A. H. (1995). On the derivation of kernels for kernel-driven models of bidirectional reflectance. *Journal of Geophysical Research*, *100*, 21077. https://doi.org/10.1029/95JD02371

Weiss, M., Baret, F., Smith, G. J., Jonckheere, I., & Coppin, P. (2004). Review of methods for in situ leaf area index (LAI) determination. *Agricultural & Forest Meteorology*, *121*, 37–53. https://doi.org/10.1016/j.agrformet.2003.08.001

Weyermann, J., Kneubühler, M., Schläpfer, D., & Schaepman, M. E. (2015). Minimizing reflectance anisotropy effects in airborne spectroscopy data using Ross-Li model inversion with continuous field land cover stratification. *IEEE Transactions on Geoscience and Remote Sensing*, *53*, 5814–5823. https://doi.org/10.1109/TGRS.2015.2415872

Whitehead, D. (1978). The estimation of foliage area from sapwood basal area in Scots pine. *Forestry*, *51*(2), 137–149. https://doi.org/10.1093/forestry/51.2.137

Zarnetske, P. L., Read, Q. D., Record, S., Gaddis, K. D., Pau, S., Hobi, M. L., Malone, S. L., Costanza, J., M. Dahlin, K., Latimer, A. M., Wilson, A. M., Grady, J. M., Ollinger, S. V., & Finley, A. O. (2019). Towards connecting biodiversity and geodiversity across scales with satellite remote sensing. *Global Ecology and Biogeography*, *28*, 548–556. https://doi.org/10.1111/geb.12887

Zhao, K., & Popescu, S. (2009). Lidar-based mapping of leaf area index and its use for validating GLOBCARBON satellite LAI product in a temperate forest of the southern USA. *Remote Sensing of Environment*, *113*, 1628–1645. https://doi.org/10.1016/j.rse.2009.03.006

Zhao, Y., Zeng, Y., Zheng, Z., Dong, W., Zhao, D., Wu, B., & Zhao, Q. (2018). Forest species diversity mapping using airborne LiDAR and hyperspectral data in a subtropical forest in China. *Remote Sensing of Environment*, *213*, 104–114. https://doi.org/10.1016/j.rse.2018.05.014

BIOSKETCH

This research team aims to better understand and quantify ecosystem processes and forest diversity through the fusion of emerging technologies, including air- and space-borne remote sensing and spatial statistics, with in situ data. They are interested in refining our understanding of ecosystem function and biodiversity to improve our ability to predict how ecosystems will change in the future.

APPENDIX A. Field site names and locations, abbreviations, and attributes, listed from South to North

Name and state	Abbr.	Latitude (°)	Elev. (m)	MAP (mm)	MAT (c)	MCH (m)	Area (km^2)	Collection dates	Lidar system
Harvard Forest, Massachusetts	HARV	42.54	351	967	8	26	340	28 August–5 September 2018	Gemini
Smithsonian Environmental Research Center, Maryland	SERC	38.89	15	1,107	14	38	110	31 July 2017	Gemini
Mountain Lake Biological Station, Virginia	MLBS	37.38	1,126	1,030	13	18	170	15 June 2018	Riegl
Oak Ridge National Laboratory, Tennessee	ORNL	35.96	334	1,222	15	28	355	11 May–13 May 2018	Riegl
Talladega National Forest, Alabama	TALL	32.95	135	1,350	17	25	150	27 April–30 April 2018	Riegl

Note: Collection dates refer to when the National Ecological Observatory Network Airborne Observation Platform (NEON AOP) collected airborne remote sensing data; Lidar system refers to the lidar sensor brand.

Abbreviations: MAP, mean annual precipitation (mm); MAT, mean annual temperature (°C); MCH, mean canopy height (m); Area, total area of AOP collection (km^2).

APPENDIX B. Functional traits and phylogeny used in this study

Trait	Unit	References
Bark thickness	cm	Kattge et al. (2020), Stevens et al. (2020)
Specific leaf area	mm^2/mg	Kattge et al. (2020), Stevens et al. (2020)
Leaf N content by mass	mg/g	Kattge et al. (2020), Stevens et al. (2020)
Leaf P content by mass	mg/g	Kattge et al. (2020), Stevens et al. (2020)
Leaf thickness	mm^2/mg	Kattge et al. (2020), Stevens et al. (2020)
Stomatal conductance per unit leaf area	mmol m^2/s	Kattge et al. (2020), Stevens et al. (2020)
Photosynthetic rate per unit leaf area	μmol m/s	Kattge et al. (2020), Stevens et al. (2020)
Specific stem density (wood density)	mg/mm^3	Kattge et al. (2020), Stevens et al. (2020)
Seed dry mass	mg	Kattge et al. (2020), Stevens et al. (2020)
Rooting depth	m	Kattge et al. (2020), Stevens et al. (2020)
Maximum life span	years	Kattge et al. (2020), Stevens et al. (2020)
Tree species phylogeny	NA	Potter and Koch (2014); Potter and Woodall (2012)

APPENDIX C. Hyperspectral variables used in this study

Variable	Abbreviation	Description	References
Convex hull volume	CHV	Range based spectral diversity metric generated from the smallest possible convex hull volume within a plot	Dahlin et al. (2016)
Sum of squares	SS	Variance based spectral diversity metric generated from the sum of the total spectral variance of the principal components	Laliberté et al. (2020)
Total variance	TV	Variance based spectral diversity metric describing the total spectral variance of the principal components	Dahlin et al. (2016)
Principal component 1	PC1	Value of the first principal component	Oldeland et al. (2010)
Principal component 2	PC2	Value of the second principal component	Oldeland et al. (2010)
Coefficient of variation	CV	Variance based spectral diversity metric based on the relative variability of reflectance measurements within a plot	Gholizadeh et al., 2019
Normalized difference vegetation index	NDV	Vegetation health remote sensing index	Rouse et al. (1974)
Photochemical reflectance index	PRI	Light use efficiency remote sensing index	Gamon et al. (1992)
Red-edge vegetation stress index	RVS	Plant stress remote sensing index	Merton and Huntington (1999)
Red-edge normalized difference vegetation index	RND	Vegetation health remote sensing index	Gitelson and Merzlyak (1994)
Shortwave infrared 1 mean reflectance	SW1	Mean reflectance of wavelengths from 1,500 to 1,800 nm	Ollinger (2011)
Shortwave infrared 2 mean reflectance	SW2	Mean reflectance of wavelengths from 2,000 to 2,400 nm	Ollinger (2011)
Near infrared mean reflectance	NIR	Mean reflectance of wavelengths from 800 to 1,350 nm	Ollinger (2011)

APPENDIX D. Lidar derived variables used in this study

Variable	Abbreviation	Description	References
Canopy height	CH	Height (m) of canopy within a given pixel	Lefsky et al. (1999)
Canopy empty volume	EV	Volume of the space within the canopy that does not contain plant material	Lefsky et al. (1999)
Canopy euphotic depth	ED	Depth (m) of the uppermost 65% of plant material within the canopy	Lefsky et al. (1999)
Canopy euphotic leaf area	ELA	Total amount of plant material within the uppermost 65% of plant material within the canopy	Lefsky et al. (1999)
Canopy euphotic volume	CEV	Volume of the uppermost 65% of plant material within the canopy	Lefsky et al. (1999)
Canopy filled voxel ratio	FVR	Ratio (%) of voxels within a column of the canopy that contain plant material	Hardiman et al. (2013)
Leaf area index	LAI	The one-sided leaf area per unit of ground area	Chen and Black (1992)
Maximum leaf area density	MLA	Largest leaf area density measurement within a column of the canopy	Hardiman et al. (2013)
Maximum leaf area density height	LAH	Height (m) of the largest leaf area density measurement within a column of the canopy	Hardiman et al. (2013)
Mean leaf area density height	LAM	Mean height (m) of the total amount of leaf material within a column of the canopy	Hardiman et al. (2013)
Canopy oligophotic leaf area	OLA	Total amount of plant material within the bottommost 35% of plant material within the canopy	Lefsky et al. (1999)

Variable	Abbreviation	Description	References
Canopy oligophotic volume	COV	Volume of the bottommost 35% of plant material within the canopy	Lefsky et al. (1999)
Canopy porosity ratio	CPR	Ratio (%) of voxels within a column of the canopy that do not contain plant material	Hardiman et al. (2013)
Leaf area density 10th quantile	L10	Height (m) of the 10th quantile of leaf material within a column of the canopy	Shi et al. (2018)
Leaf area density 25th quantile	L25	Height (m) of the 25th quantile of leaf material within a column of the canopy	Shi et al. (2018)
Leaf area density 50th quantile	L50	Height (m) of the 50th quantile of leaf material within a column of the canopy	Shi et al. (2018)
Leaf area density 75th quantile	L75	Height (m) of the 75th quantile of leaf material within a column of the canopy	Shi et al. (2018)
Leaf area density 90th quantile	L90	Height (m) of the 90th quantile of leaf material within a column of the canopy	Shi et al. (2018)
Standard deviation of leaf area density	LSD	The standard deviation of the leaf area density measurement within a column of the canopy	Hardiman et al. (2011)
Top of canopy rugosity	CR	Sum of the intercell difference between the central cell and their CH_{lidar} measurements converted to a volume	Lefsky et al. (1999)
Within canopy rugosity	WIC	The standard deviation of the central cell and the eight surrounding pixels based on their LAD_{SD} measurement	Hardiman et al. (2011)
Leaf Area Density	LAD	The total leaf area per unit of volume	Weiss et al. (2004)

APPENDIX E. Topographic variables used in this study

	Variable	Abbreviation	Description	References
Topographic variable	Digital surface model	DSM	Elevation (m) of all objects on Earth's surface	QGIS, 2022
	Digital terrain model	DTM	Elevation (m) of the Earth's surface	QGIS, 2022
	Eastness	EAS	How eastward a pixel's slope is facing: derived from sin(aspect)	QGIS, 2022
	Latitude	LAT	Latitude (°) of the pixel centroid	QGIS, 2022
	Longitude	LON	Longitude (°) of the pixel centroid	QGIS, 2022
	Northness	NOR	How northward a pixel is: derived from cos(aspect)	QGIS, 2022
	Slope	SLO	Slope of pixel (°)	QGIS, 2022
	Topographic position index	TPI	The intercell difference between the central cell and the mean of the eight surrounding cells	QGIS, 2022
	Topographic roughness index	TRI	The mean difference between the central cell and the eight surrounding cells	QGIS, 2022

APPENDIX F. Beer–Lambert coefficients

Site	Year	Beer–Lambert coefficient
TALL	2018	.4982
ORNL	2018	.8354
MLBS	2018	.8776
SERC	2017	.6784
HARV	2018	.7796

APPENDIX G. Results from all individual models

	Sensor	Marginal R^2	Conditional R^2	Root Mean Square Error (RMSE)	AIC	Variable	Coefficient
Taxonomic diversity	All	.46	.46	.36	122.7	Maximum Leaf Area Density Height - Range	.3308
						Principal Component 1 - Min	−.2982
						Canopy Filled Voxel Ratio - SD	−.4171
						Digital Surface Model - SD	.1972
						Within Canopy Rugosity - SD	.1874
						Slope - Min	−.1724
						Eastness - Mean	.2081
	HSI	.13	.13	.46	144.9	Near Infrared Mean Reflectance - SD	.3268
						Principal Component 1 - SD	−.2681
	Lidar	.41	.41	.38	126.3	Maximum Leaf Area Density Height - Range	.3144
						Canopy Filled Voxel Ratio - SD	−.4086
						Canopy Euphotic Leaf Area - Min	.2446
						Leaf Area Density 90th Quantile - SD	.2686
						Within Canopy Rugosity - Min	−.2167
						Canopy Filled Voxel Ratio - Max	−.1804
	Topography	.09	.18	.46	148.6	Digital Surface Model - SD	.2609
						Slope - Min	−.2990
Phylogenetic diversity	All	.33	.70	.36	123.7	Maximum Leaf Area Density Height - Range	.3004
						Topograhic Roughness Index - Min	−.2610
						Normalized Difference Vegetation Index - Mean	.5557
						Red-Edge Normalized Difference Vegetation Index - SD	.2823
	HSI	.29	.50	.39	130.3	Principal Component 2 - Min	−.3275
						Normalized Difference Vegetation Index - Mean	.7163
						Red-Edge Normalized Difference Vegetation Index - SD	.3737
						Photochemical Reflectance Index - Range	−.3438
	Lidar	.19	.38	.41	133.5	Canopy Euphotic Leaf Area - Min	.2785
						Maximum Leaf Area Density Height - Range	.2936
	Topography	.17	.30	.42	136.1	Topographic Position Index - Mean	−.2649
						Topographic Rougness Index - Min	−.3200
Functional diversity	All	.31	.31	.41	131.9	Maximum Leaf Area Density Height - Range	.3336
						Canopy Porosity Ratio - SD	−.2451
						Principal Component 1 - Min	−.3058
						Slope - Min	−.1884
	HSI	.13	.14	.46	140.5	Principal Component 1 - Min	−.3632
	Lidar	.22	.27	.43	133.5	Maximum Leaf Area Density Height - Range	.4103
						Canopy Porosity Ratio - SD	−.3147
	Topography	.06	.13	.47	147.8	Slope - Min	−.2483

Abbreviation: AIC, akaike information criterion.

Additional information about variables available in Appendices C-E.

APPENDIX H. Missing species per trait

Trait	Number of species	Number of missing species	Percent of traits missing
Bark Thickness	60	8	13.3%
Leaf Nitrogen	60	9	15%
Leaf Phosphorus	60	9	15%
Leaf Photosynthetic Area	60	20	33.3%
Leaf Thickness	60	26	43.3%
Plant Life Span	60	27	45%
Rooting Depth	60	9	15%
Seed Dry Mass	60	8	13.3%
Specific Leaf Area	60	11	18.3%
Stem Specific Density	60	10	16.7%
Stomata Conductance Area	60	26	43.3%

Additional information about each trait in Appendix B.